THE LUBRICATION OF PARALLEL SURFACE THRUST BEARINGS

by

IAIN GEORGE CURRIE

A THESIS SUBMITTED IN PARTIAL FULFILMENT OF THE REQUIREMENTS

FOR THE DEGREE OF MASTER OF APPLIED SCIENCE

in the Department

of

MECHANICAL ENGINEERING

We accept this thesis as conforming to the required standard

THE UNIVERSITY OF BRITISH COLUMBIA

MAY, 1962

In presenting this thesis in partial fulfilment of the requirements for an advanced degree at the University of British Columbia, I agree that the library shall make it freely available for reference and study. I further agree that permission for extensive copying of this thesis for scholarly purposes may be granted by the Head of my Department or by his representatives. It is understood that copying of this thesis for financial gain shall not be allowed without my written permission.

Department of Mechanical Engineering
The University of British Columbia,
Vancouver 8, Canada.

May, 1962.

ABSTRACT

The parallel surface thrust bearing has been studied both theoretically and experimentally. The general equations governing the laminar flow of a Newtonian fluid are presented and suitably reduced to describe the flow of lubricant through a plain collar bearing. A computer solution of the resulting equations has been obtained in which the variations of density and viscosity with temperature are accommodated and the circumferential leakage of oil from the bearing is recognised. The resulting performance curves indicate that useful load carrying capacities, produced by a 'thermal wedge' effect, are possible with parallel surface thrust bearings.

A series of tests was carried out on a three inch diameter bearing operating at speeds ranging from 15,000 to 19,000 r.p.m. The results confirm that hydrodynamic lubrication may be achieved with a parallel surface thrust bearing. The experimental values obtained for the load carrying capacity and the coefficient of friction were both less than the theoretical predictions. The discrepancies appear to be caused, for the most part, by an increase in the oil temperature resulting from entrainment of the lubricant in the bearing.

ACKNOWLEDGEMENT

TABLE OF CONTENTS

LIST OF FIGURES

LIST OF SYMBOLS

The following symbols have been used throughout the text.

Any symbol not listed is defined on introduction.

r, θ, ζ	Independent cylindrical co-ordinates
x, y, ζ	Independent rectangular co-ordinates
u, v, w	Velocity in x, y and ζ direction respectively
$\frac{D}{Dt'}$	Substantial time derivative
a	Grid size
A	Constant
B	Constant
C_p	Specific heat at constant pressure
C_v	Specific heat at constant volume
D	Dimensionless density
E	Internal energy
f	Coefficient of friction
$\vec{F}$	Body force, direction as subscripted
F_f	Friction force
h	Film thickness
H	Enthalpy
k	Thermal conductivity
M	Dimensionless viscosity
N	Rotational speed
p	Pressure
P	Dimensionless pressure
P'	Load per unit area
$\vec{q}$	Heat flux, direction as subscripted
r_o	Inner radius of bearing
r_i	Outer radius of bearing
r_m	Mean radius of bearing
R	Dimensionless co-ordinate
t	Temperature
t_o	Temperature at inlet
t'	Time
T	Dimensionless temperature
T_f	Friction torque
U	Velocity of slider
$\vec{v}$	Velocity, direction as subscripted
W	Load per pad
Z	Viscosity in centipoise
α	Included angle of sector pad
β	Constant
Δ	Dilatation $= \nabla \cdot \vec{v}$
∇	Operator
Θ	Dimensionless co-ordinate
λ	Constant

μ	Viscosity
μ_o	Viscosity at inlet
ρ	Density
ρ_o	Density at inlet
τ	Stress tensor
ϕ	Dissipation function
ω	Angular velocity

CHAPTER I

I. 1. Introduction

I.1. Introduction

Prior to, and for some time subsequent to the introduction of Reynolds' classical paper [1]* in 1886, thrust bearings were very inefficient when compared to the journal bearing. In his quantitative analysis, Reynolds showed that a geometric restriction in the direction of motion was necessary to produce a load carrying fluid film in a bearing. The parallel surface thrust bearing, which at that time was operating at low speed and with high loads imposed on it, had no such geometric restriction. Due to these severe running conditions and the lack of oil grooves, or other means of aiding oil entry to the bearing surfaces, the thrust bearing was then operating in the boundary lubrication region. By fortuitous coincidence, however, the journal bearing already possessed the geometry required for hydrodynamic lubrication and so operated with a lower coefficient of friction than the thrust bearing.

As a consequence of Reynolds' theory, thrust bearings of the early twentieth century, and later, were designed on the tilting pad principle, as introduced by Kingsbury and Michell, and the parallel surface bearing became virtually obsolete. The contention was that the latter bearing could support a fluid film under load only to the extent of the static pressure.

On several occasions, however, it was noted that parallel surface bearings performed better than expected inasmuch as useful loads were carried with a low coefficient of friction. The most conclusive results were obtained by Fogg [2] who recorded load carrying capacities of the same order as a tilting pad bearing with almost the same efficiency as the tilting pad bearing. His tests were carried out at comparatively high speeds and the annular thrust surfaces were divided into a number of sector shaped pads

* Numbers in square brackets refer to list of references in Bibliography.

by the introduction of radial oil grooves in the stationary surfaces.
These oil grooves, together with circumferential oil seals, ensured that the
bearing surfaces were always supplied with oil.

Fogg explained this apparent hydrodynamic action as a 'thermal
wedge' effect, analagous to the taper wedge effect which predominated in the
tilting pad bearings.   That is, instead of having a constant volume of
lubricant flowing through a diminishing area, Fogg postulated that due to the
thermal expansion of the lubricant a similar effect would be obtained by an
expanding volume of lubricant flowing through a constant area.

As a result of Fogg's findings, more attention was given to
the parallel surface thrust bearing, most of this attention being
quantitative in nature.

Bower [3] used the equation of mass continuity, as opposed to
volume continuity, in a revised form of the governing equation.   By assuming
no side leakage and linear variations of viscosity and density along the
bearing, Bower concluded that a load carrying fluid film could be produced by
the thermal wedge effect.

Cameron and Wood [4] used the revised form of Reynolds'
equation in conjunction with an energy equation to arrive at two simultaneous
partial differential equations for the pressure and temperature distributions.
Using mathematically expressed variations of viscosity and density with
temperature, these equations were then solved on the assumption of no side
leakage from the bearing.

Shaw [5] obtained a solution to the revised governing
equation by assuming no side leakage, constant viscosity and a linear
variation of density with temperature.   In this way he was able to compare
the tilting pad and the parallel surface bearings on the basis of equal film
thicknesses.

Starting with the general equations for the steady flow of a viscous fluid, Cope [6] arrived at the revised form of the pressure equation, but obtained an energy equation which differed from that used previously by Cameron and Wood. The resulting equations were solved by Cope for known variations of viscosity and density with temperature and for no side leakage. In this way he showed that under conditions of low variation of viscosity with temperature, large variation of density with temperature, and small film thicknesses, the thermal wedge may completely outclass the geometric wedge.

Experimental results were obtained by Kettleborough [7] for a parallel surface bearing running at the comparatively low speed of 695 r.p.m. The coefficient of friction so obtained was about twice that obtained by Fogg.

The work performed on parallel surface bearings has tended to be either entirely experimental or entirely theoretical, the theoretical analyses being used only to justify the thermal wedge idea and to compare the performance of such a bearing to that of a similar tilting pad type. The first real attempt to correlate theoretical and experimental results for a given parallel surface bearing was due to Young [8]. In his quantitative analysis, Young presented three different solutions to the equations as presented by Cope, the most rigorous solution being a relaxation process, first used in lubrication by Christopherson [9], which takes account of side leakage. These different solutions were compared with each other and with the experimental results obtained from a thrust bearing operating in the speed range 4,000 to 16,000 r.p.m. The relaxation solution gave fairly good agreement at the points checked but theoretical performance curves could not be obtained this way due to the large amount of work involved in even one solution. The experimental coefficients of friction were higher than those obtained by Fogg, but lower than those obtained by Kettleborough.

The validity of the assumptions which accompany the

theoretical analysis of the fluid flow in a parallel surface thrust bearing, evidently depends on the nature of the operating conditions in the test bearing itself. Also, the theoretical results obtained can be successfully compared with the experimental results only if certain quantities can be accurately measured. It thus seems desirable to revise, and modify if necessary, the equations governing the flow of fluid in a parallel surface bearing; to obtain as sophisticated a solution to the governing equations as is reasonable; to add to the experimental data available and to compare the theoretical and experimental results so obtained. It was with these immediate objectives that the current research program was initiated.

CHAPTER   II

II.1. The Governing Equations for Film Lubrication

The equations governing the flow of the lubricant in a parallel surface bearing will be obtained from the general equations governing the flow of a viscous, compressible, heat conducting fluid. The derivation of these general equations is presented in most texts on hydrodynamics, gasdynamics and related fields. Accordingly, the general equations as presented in [10] are:-

$$\frac{D\rho}{Dt'} = -\rho(\nabla \cdot \vec{v}) \qquad . \qquad . \quad (1)$$

$$\rho\frac{D\vec{v}}{Dt'} = \rho\vec{F} - \nabla p - [\nabla \cdot \vec{\tau}] \qquad . \qquad . \quad (2)$$

$$\rho\frac{DH}{Dt'} = \frac{Dp}{Dt'} - (\nabla \cdot \vec{q}) - (\tau : \nabla\vec{v}) \qquad . \qquad . \quad (3)$$

in which the symbols used are defined in the 'List of Symbols' in the preliminary pages of the thesis. These are the equations of continuity, motion and energy, respectively, in which the properties of the fluid are variables.

The reduction of these general equations to their final form will be carried out by the method presented by Cope [6], although the resulting equations will be slightly different. The algebraic manipulations, although straightforward, tend to become lengthy and tedious. Consequently, it is proposed to indicate the steps individually and to present the end results of performing each step.

We begin by expanding equations (1), (2) and (3) in cylindrical co-ordinates:

$$\frac{\partial\rho}{\partial t'} + v_r\frac{\partial\rho}{\partial r} + \frac{v_\theta}{r}\frac{\partial\rho}{\partial\theta} + v_3\frac{\partial\rho}{\partial 3} = -\rho\left[\frac{1}{r}\frac{\partial}{\partial r}(rv_r) + \frac{1}{r}\frac{\partial v_\theta}{\partial\theta} + \frac{\partial v_3}{\partial 3}\right] \qquad . \qquad . \quad (4)$$

$$\rho\left(\frac{\partial v_r}{\partial t'} + v_r\frac{\partial v_r}{\partial r} + \frac{v_\theta}{r}\frac{\partial v_r}{\partial\theta} - \frac{v_\theta^2}{r} + v_3\frac{\partial v_r}{\partial 3}\right) = \rho F_r - \frac{\partial p}{\partial r} - \left[\frac{1}{r}\frac{\partial}{\partial r}(r\tau_{rr}) + \frac{1}{r}\frac{\partial\tau_{r\theta}}{\partial\theta} - \frac{\tau_{\theta\theta}}{r} + \frac{\partial\tau_{r3}}{\partial 3}\right]$$

$$\rho\left(\frac{\partial v_\theta}{\partial t'} + v_r\frac{\partial v_\theta}{\partial r} + \frac{v_\theta}{r}\frac{\partial v_\theta}{\partial\theta} + \frac{v_r v_\theta}{r} + v_3\frac{\partial v_\theta}{\partial 3}\right) = \rho F_\theta - \frac{1}{r}\frac{\partial p}{\partial\theta} - \left[\frac{1}{r^2}\frac{\partial}{\partial r}(r^2\tau_{r\theta}) + \frac{1}{r}\frac{\partial\tau_{\theta\theta}}{\partial\theta} + \frac{\partial\tau_{\theta 3}}{\partial 3}\right] \qquad \left.\right\} \quad . \quad (5)$$

$$\rho\left(\frac{\partial v_3}{\partial t'} + v_r\frac{\partial v_3}{\partial r} + \frac{v_\theta}{r}\frac{\partial v_3}{\partial\theta} + v_3\frac{\partial v_3}{\partial 3}\right) = \rho F_3 - \frac{\partial p}{\partial 3} - \left[\frac{1}{r}\frac{\partial}{\partial r}(r\tau_{r3}) + \frac{1}{r}\frac{\partial\tau_{\theta 3}}{\partial\theta} + \frac{\partial\tau_{33}}{\partial 3}\right]$$

$$\rho\left(\frac{\partial H}{\partial t'} + v_r\frac{\partial H}{\partial r} + \frac{v_\theta}{r}\frac{\partial H}{\partial\theta} + v_3\frac{\partial H}{\partial 3}\right) = \left(\frac{\partial p}{\partial t'} + v_r\frac{\partial p}{\partial r} + \frac{v_\theta}{r}\frac{\partial p}{\partial\theta} + v_3\frac{\partial p}{\partial 3}\right) -$$
$$\left[\frac{1}{r}\frac{\partial}{\partial r}(rq_r) + \frac{1}{r}\frac{\partial q_\theta}{\partial\theta} + \frac{\partial q_3}{\partial 3}\right] + \phi \qquad . \qquad . \quad (6)$$

in which the components of the heat flux vector $\vec{q}$ are given by:

$$
\left.
\begin{array}{l}
q_r = -k\dfrac{\partial t}{\partial r} \\[2mm]
q_\theta = -k\dfrac{1}{r}\dfrac{\partial t}{\partial\theta} \\[2mm]
q_3 = -k\dfrac{\partial t}{\partial_3}
\end{array}
\right\}
\qquad\qquad . \qquad . \quad (7)
$$

For a Newtonian fluid we have:

$$
\left.
\begin{array}{l}
\tau_{rr} = -\mu\left(2\dfrac{\partial v_r}{\partial r} - \dfrac{2}{3}\Delta\right) \\[2mm]
\tau_{\theta\theta} = -\mu\left[2\left(\dfrac{1}{r}\dfrac{\partial v_\theta}{\partial\theta} + \dfrac{v_r}{r}\right) - \dfrac{2}{3}\Delta\right] \\[2mm]
\tau_{33} = -\mu\left(2\dfrac{\partial v_3}{\partial_3} - \dfrac{2}{3}\Delta\right) \\[2mm]
\tau_{r\theta} = \tau_{\theta r} = -\mu\left[r\dfrac{\partial}{\partial r}\left(\dfrac{v_\theta}{r}\right) + \dfrac{1}{r}\dfrac{\partial v_r}{\partial\theta}\right] \\[2mm]
\tau_{\theta 3} = \tau_{3\theta} = -\mu\left(\dfrac{\partial v_\theta}{\partial_3} + \dfrac{1}{r}\dfrac{\partial v_3}{\partial\theta}\right) \\[2mm]
\tau_{3r} = \tau_{r3} = -\mu\left(\dfrac{\partial v_3}{\partial r} + \dfrac{\partial v_r}{\partial_3}\right)
\end{array}
\right\}
\qquad . \qquad . \quad (8)
$$

$$
\phi = \mu\left\{2\left[\left(\dfrac{\partial v_r}{\partial r}\right)^2 + \left(\dfrac{1}{r}\dfrac{\partial v_\theta}{\partial\theta} + \dfrac{v_r}{r}\right)^2 + \left(\dfrac{\partial v_3}{\partial_3}\right)^2\right] + \left[r\dfrac{\partial}{\partial r}\left(\dfrac{v_\theta}{r}\right) + \dfrac{1}{r}\dfrac{\partial v_r}{\partial\theta}\right]^2 + \right.
$$
$$
\left. \left[\dfrac{1}{r}\dfrac{\partial v_3}{\partial\theta} + \dfrac{\partial v_\theta}{\partial_3}\right]^2 + \left[\dfrac{\partial v_r}{\partial_3} + \dfrac{\partial v_3}{\partial r}\right]^2 - \dfrac{2}{3}\Delta^2\right\} \qquad . \qquad . \quad (9)
$$

Thus assuming the flow is steady and laminar and that the fluid is Newtonian, the general equations (4), (5) and (6) become:

$$
\dfrac{1}{r}\dfrac{\partial}{\partial r}\left(\rho r v_r\right) + \dfrac{1}{r}\dfrac{\partial}{\partial\theta}\left(\rho v_\theta\right) + \dfrac{\partial}{\partial_3}\left(\rho v_3\right) = 0 \qquad . \qquad . \quad (10)
$$

$$
\left.
\begin{array}{l}
\rho\left(v_r\dfrac{\partial v_r}{\partial r} + \dfrac{v_\theta}{r}\dfrac{\partial v_r}{\partial\theta} - \dfrac{v_\theta^2}{r} + v_3\dfrac{\partial v_r}{\partial_3}\right) = \rho F_r - \dfrac{\partial p}{\partial r} + \mu\nabla^2 v_r + \dfrac{\mu}{3}\dfrac{\partial\Delta}{\partial r} - \dfrac{2\mu}{r^2}\left(v_r + \dfrac{\partial v_\theta}{\partial\theta}\right) + \\[2mm]
\qquad \dfrac{4}{3}\dfrac{\partial\mu}{\partial r}\dfrac{\partial v_r}{\partial r} - \dfrac{2}{3}\dfrac{\partial\mu}{\partial r}\left(\dfrac{v_r}{r} + \dfrac{1}{r}\dfrac{\partial v_\theta}{\partial\theta} + \dfrac{\partial v_3}{\partial_3}\right) + \\[2mm]
\qquad \dfrac{\partial\mu}{\partial\theta}\left[\dfrac{\partial}{\partial r}\left(\dfrac{v_\theta}{r}\right) + \dfrac{1}{r^2}\dfrac{\partial v_r}{\partial\theta}\right] + \dfrac{\partial\mu}{\partial_3}\left(\dfrac{\partial v_3}{\partial r} + \dfrac{\partial v_r}{\partial_3}\right) \\[4mm]
\rho\left(v_r\dfrac{\partial v_\theta}{\partial r} + \dfrac{v_\theta}{r}\dfrac{\partial v_\theta}{\partial\theta} + \dfrac{v_r v_\theta}{r} + v_3\dfrac{\partial v_\theta}{\partial_3}\right) = \rho F_\theta - \dfrac{1}{r}\dfrac{\partial p}{\partial\theta} + \mu\nabla^2 v_\theta + \dfrac{\mu}{3}\dfrac{1}{r}\dfrac{\partial\Delta}{\partial\theta} - \dfrac{\mu}{r^2}\left(v_\theta - 2\dfrac{\partial v_r}{\partial\theta}\right) + \\[2mm]
\qquad \dfrac{\partial\mu}{\partial r}\left[r\dfrac{\partial}{\partial r}\left(\dfrac{v_\theta}{r}\right) + \dfrac{1}{r}\dfrac{\partial v_r}{\partial\theta}\right] + \dfrac{4}{3r^2}\dfrac{\partial\mu}{\partial\theta}\left(v_r + \dfrac{\partial v_\theta}{\partial\theta}\right) - \\[2mm]
\qquad \dfrac{2}{3r}\dfrac{\partial\mu}{\partial\theta}\left(\dfrac{\partial v_r}{\partial r} + \dfrac{\partial v_3}{\partial_3}\right) + \dfrac{\partial\mu}{\partial_3}\left(\dfrac{\partial v_\theta}{\partial_3} + \dfrac{1}{r}\dfrac{\partial v_3}{\partial\theta}\right) \\[4mm]
\rho\left(v_r\dfrac{\partial v_3}{\partial r} + \dfrac{v_\theta}{r}\dfrac{\partial v_3}{\partial\theta} + v_3\dfrac{\partial v_3}{\partial_3}\right) = \rho F_3 - \dfrac{\partial p}{\partial_3} + \mu\nabla^2 v_3 + \dfrac{\mu}{3}\dfrac{\partial\Delta}{\partial_3} + \dfrac{1}{r}\dfrac{\partial\mu}{\partial r}\left(\dfrac{\partial v_3}{\partial r} + \dfrac{\partial v_r}{\partial_3}\right) + \\[2mm]
\qquad \dfrac{1}{r}\dfrac{\partial\mu}{\partial\theta}\left(\dfrac{\partial v_\theta}{\partial_3} + \dfrac{1}{r}\dfrac{\partial v_3}{\partial\theta}\right) + \dfrac{4}{3}\dfrac{\partial\mu}{\partial_3}\dfrac{\partial v_3}{\partial_3} - \\[2mm]
\qquad \dfrac{2}{3}\dfrac{\partial\mu}{\partial_3}\left(\dfrac{\partial v_r}{\partial r} + \dfrac{v_r}{r} + \dfrac{1}{r}\dfrac{\partial v_\theta}{\partial\theta}\right)
\end{array}
\right\}(11)
$$

$$
\rho\left(v_r\dfrac{\partial H}{\partial r} + \dfrac{v_\theta}{r}\dfrac{\partial H}{\partial\theta} + v_3\dfrac{\partial H}{\partial_3}\right) = \left(v_r\dfrac{\partial p}{\partial r} + \dfrac{v_\theta}{r}\dfrac{\partial p}{\partial\theta} + v_3\dfrac{\partial p}{\partial_3}\right) +
$$
$$
\left[\dfrac{1}{r}\dfrac{\partial}{\partial r}\left(k r\dfrac{\partial t}{\partial r}\right) + \dfrac{1}{r}\dfrac{\partial}{\partial\theta}\left(\dfrac{k}{r}\dfrac{\partial t}{\partial\theta}\right) + \dfrac{\partial}{\partial_3}\left(k\dfrac{\partial t}{\partial_3}\right)\right] + \phi \quad . \quad (12)
$$

in which the continuity equation (10) has been rearranged to its more usual form.

Since the surfaces in a bearing are close together, parallel and in relative tangential motion, it is reasonable to assume:

(i) That the variation of pressure, density, temperature, viscosity and thermal conductivity across the film are far less important than their variation along it. That is, it is assumed that

p, ρ, t, μ and k are functions of r and θ only.

(ii) That the velocity gradients across the film are much more important than velocity gradients parellel to it. Symbolically, this assumption states that

$$\frac{\partial v_\theta}{\partial \mathfrak{z}} \gg \frac{\partial v_\theta}{\partial \theta} \, , \qquad \frac{\partial^2 v_\theta}{\partial \mathfrak{z}^2} \gg \frac{\partial^2 v_\theta}{\partial \mathfrak{z} \partial \theta} \gg \frac{\partial^2 v_\theta}{\partial \theta^2}$$

and so on, so that only the first named need be retained in groups of such terms.

(iii) That the fluid velocity perpendicular to the film is very small so that we may write

$$v_{\mathfrak{z}} = 0$$

(iv) That the body forces, other than those caused by the motion of the fluid, are negligible. Using the notation adopted, the assumption means that

$$F_r = F_\theta = F_{\mathfrak{z}} = 0$$

(v) That the enthalpy of the fluid is a function of temperature only and that the specific heat remains constant. Consequently, we may write

$$H = C_p t$$

Applying these five assumptions to equations (10), (11) and (12), they reduce to the form:

$$\frac{1}{r} \frac{\partial}{\partial r} \left(\rho r v_r \right) + \frac{1}{r} \frac{\partial}{\partial \theta} \left(\rho v_\theta \right) = 0 \qquad\qquad \text{(13)}$$

$$\rho\left(v_r \frac{\partial v_r}{\partial r} + \frac{v_\theta}{r}\frac{\partial v_r}{\partial \theta} - \frac{v_\theta^2}{r}\right) = -\frac{\partial p}{\partial r} + \mu \frac{\partial^2 v_r}{\partial z^2} \left.\begin{array}{c} \\ \\ \end{array}\right\}$$

$$\rho\left(v_r \frac{\partial v_\theta}{\partial r} + \frac{v_\theta}{r}\frac{\partial v_\theta}{\partial \theta} + \frac{v_r v_\theta}{r}\right) = -\frac{1}{r}\frac{\partial p}{\partial \theta} + \mu \frac{\partial^2 v_\theta}{\partial z^2} \qquad (14)$$

$$\rho C_p\left(v_r \frac{\partial t}{\partial r} + \frac{v_\theta}{r}\frac{\partial t}{\partial \theta}\right) = \left(v_r \frac{\partial p}{\partial r} + \frac{v_\theta}{r}\frac{\partial p}{\partial \theta}\right) + \left[\frac{1}{r}\frac{\partial}{\partial r}\left(kr\frac{\partial t}{\partial r}\right) + \frac{1}{r}\frac{\partial}{\partial \theta}\left(\frac{k}{r}\frac{\partial t}{\partial \theta}\right)\right] +$$
$$\mu\left[\left(\frac{\partial v_\theta}{\partial z}\right)^2 + \left(\frac{\partial v_r}{\partial z}\right)^2\right] \qquad (15)$$

These equations are still rather elaborate and it is desirable to reduce them still further before attempting a solution. This can be done by using actual measurements, for a typical set of conditions, for values of ρ, p, h, etc., calculating from them the orders of magnitude of the various terms in the above equations and neglecting any terms which are found to be small. Consider, in particular, a 3 inch diameter bearing running at 15,000 r.p.m. with a light lubricating oil at a temperature of 150°F and film thickness of 0.001 inch. These figures are estimated for the test bearing to be used. For these conditions Table I is compiled in which all quantities have been converted to the units of lbs., ft., secs., and °F.

TABLE I

ρ	p	h	μ	C_p	k	r	t	ωr
1.614	3000	0.00083	0.000214	12,470	0.0173	0.1	150	143

Now $\frac{\partial v_\theta}{\partial z}$ is of the same order as $\frac{\omega r}{h}$ and $\frac{\partial^2 v_\theta}{\partial z^2}$ is of the same order as $\frac{\omega r}{h^2}$, etc..

Proceeding in this way Table II is compiled.

TABLE II

$\rho\frac{v_\theta}{r}\frac{\partial v_\theta}{\partial \theta}$	$\rho\frac{v_r v_\theta}{r}$	$\frac{1}{r}\frac{\partial p}{\partial \theta}$	$\mu\frac{\partial^2 v_\theta}{\partial z^2}$	$\rho C_p\frac{v_\theta}{r}\frac{\partial t}{\partial \theta}$	$\frac{v_\theta}{r}\frac{\partial p}{\partial \theta}$	$\frac{1}{r}\frac{\partial}{\partial \theta}\left(\frac{k}{r}\frac{\partial t}{\partial \theta}\right)$	$\mu\left(\frac{\partial v_\theta}{\partial z}\right)^2$
2×10^3	20×10^3	40×10^3	40×10^3	10×10^6	5×10^6	0.0001×10^6	5×10^6

The above Table shows that, in the equations of motion, the inertia terms $\left(\rho\frac{v_\theta}{r}\frac{\partial v_\theta}{\partial \theta} \text{ etc.}\right)$ are about one twentieth of the principal terms and may be

neglected without serious error. The force arising from the Coriolis component of acceleration $\left(\frac{v_r v_\theta}{r}\right)$ is about half that of the remaining terms. Although this term is virtually of the first order, it will be neglected here also since this approximation leads to considerable simplification of the equations, as will be shown. In any case, the pressure of 20 lbs./sq. in. assumed here is extremely modest, relative to the pressures of 2,000 lbs./sq. in. which have been recorded under smaller film thicknesses. Under conditions of large pressure gradients and shear rates, the force due to Coriolis acceleration $\left(\rho \frac{v_r v_\theta}{r}\right)$ will become insignificant. Similar considerations also apply to the centrifugal force $\left(\rho \frac{v_\theta^2}{r}\right)$.

In the energy equation, the conductivity terms $\left[\frac{1}{r}\frac{\partial}{\partial\theta}\left(\frac{k}{r}\frac{\partial t}{\partial\theta}\right) \text{ etc.}\right]$ are seen to be about 10^{-5} of the other terms and are thus negligible. The equations now become:

$$\frac{1}{r}\frac{\partial}{\partial r}\left(\rho r v_r\right) + \frac{1}{r}\frac{\partial}{\partial\theta}\left(\rho v_\theta\right) = 0 \qquad\qquad (16)$$

$$\left.\begin{aligned} 0 &= -\frac{\partial p}{\partial r} + \mu\frac{\partial^2 v_r}{\partial\zeta^2} \\ 0 &= -\frac{1}{r}\frac{\partial p}{\partial\theta} + \mu\frac{\partial^2 v_\theta}{\partial\zeta^2} \end{aligned}\right\} \qquad\qquad (17)$$

$$\rho C_p\left(v_r\frac{\partial t}{\partial r} + \frac{v_\theta}{r}\frac{\partial t}{\partial\theta}\right) = \left(v_r\frac{\partial p}{\partial r} + \frac{v_\theta}{r}\frac{\partial p}{\partial\theta}\right) + \mu\left[\left(\frac{\partial v_\theta}{\partial\zeta}\right)^2 + \left(\frac{\partial v_r}{\partial\zeta}\right)^2\right] \qquad (18)$$

In this form, the equations of motion (17) may now be integrated twice with respect to ζ to give the velocity distributions. On applying the velocity boundary conditions,

$$\text{at } \zeta = 0, \quad v_r = 0, \quad v_\theta = \omega r$$

$$\text{at } \zeta = h, \quad v_r = 0, \quad v_\theta = 0$$

the velocity expressions are found to be:

$$\left.\begin{aligned} v_r &= -\frac{1}{2\mu}\frac{\partial p}{\partial r}\zeta(h-\zeta) \\ v_\theta &= -\frac{1}{2\mu r}\frac{\partial p}{\partial\theta}\zeta(h-\zeta) + \frac{\omega r}{h}(h-\zeta) \end{aligned}\right\} \qquad\qquad (19)$$

Substitution of these expressions into the equations of continuity (16) and energy (18) yields:

$$\frac{1}{r}\frac{\partial}{\partial r}\left\{\rho r\left[-\frac{1}{2\mu}\frac{\partial p}{\partial r}\zeta(h-\zeta)\right]\right\}+\frac{1}{r}\frac{\partial}{\partial\theta}\left\{\rho\left[-\frac{1}{2\mu r}\frac{\partial p}{\partial\theta}\zeta(h-\zeta)+\frac{\omega r}{h}(h-\zeta)\right]\right\}=0 \qquad . \qquad . \quad (20)$$

$$\rho C_p\left\{\left[-\frac{1}{2\mu}\frac{\partial p}{\partial r}\zeta(h-\zeta)\frac{\partial t}{\partial r}\right]+\frac{1}{r}\left[-\frac{1}{2\mu r}\frac{\partial p}{\partial\theta}\zeta(h-\zeta)+\frac{\omega r}{h}(h-\zeta)\right]\frac{\partial t}{\partial\theta}\right\}=\left\{\left[-\frac{1}{2\mu}\frac{\partial p}{\partial r}\zeta(h-\zeta)\frac{\partial p}{\partial r}\right]+\right.$$
$$\left.\frac{1}{r}\left[-\frac{1}{2\mu r}\frac{\partial p}{\partial\theta}\zeta(h-\zeta)+\frac{\omega r}{h}(h-\zeta)\frac{\partial p}{\partial\theta}\right]\right\}+$$
$$\mu\left\{\left[-\frac{1}{2\mu r}\frac{\partial p}{\partial\theta}(h-2\zeta)-\frac{\omega r}{h}\right]^2+\left[-\frac{1}{2\mu}\frac{\partial p}{\partial r}(h-2\zeta)\right]^2\right\} \cdot \qquad . \quad (21)$$

Integrating with respect to ζ between the limits $\zeta = 0$ and $\zeta = h$ and

simplifying, we obtain the governing equations in polar co-ordinates.

$$\frac{\partial}{\partial\theta}\left(\frac{\rho}{\mu}\frac{\partial p}{\partial\theta}\right)+r\frac{\partial}{\partial r}\left(\frac{\rho}{\mu}r\frac{\partial p}{\partial r}\right)=\frac{6\omega r^2}{h^2}\frac{\partial\rho}{\partial\theta} \qquad . \qquad . \quad (22)$$

$$\rho C_p\left\{\left(\frac{\omega h}{2}-\frac{1}{r^2}\frac{h^3}{12\mu}\frac{\partial p}{\partial\theta}\right)\frac{\partial t}{\partial\theta}-\frac{h^3}{12\mu}\frac{\partial p}{\partial r}\frac{\partial t}{\partial r}\right\}=\frac{\omega^2 r^2\mu}{h}+\frac{\omega h}{2}\frac{\partial p}{\partial\theta} \qquad . \qquad . \quad (23)$$

In the absence of an equation of state for liquids, it is usual to express the

density and viscosity as functions of the pressure and temperature. In the

pressure and temperature ranges encountered, it is sufficiently accurate to

assume that both the density and viscosity are functions of the temperature

only, the variation being given by:

$$\rho = A(1-\lambda t) \qquad . \qquad . \quad (24)$$

$$\mu = B t^{-\beta} \qquad . \qquad . \quad (25)$$

Thus the equations available to solve for the pressure and temperature

distributions are:

$$\frac{\partial}{\partial\theta}\left(\frac{\rho}{\mu}\frac{\partial p}{\partial\theta}\right)+r\frac{\partial}{\partial r}\left(\frac{\rho}{\mu}r\frac{\partial p}{\partial r}\right)=\frac{6\omega r^2}{h^2}\frac{\partial\rho}{\partial\theta} \qquad\qquad (22)$$

$$\rho C_p\left\{\left(\frac{\omega h}{2}-\frac{1}{r^2}\frac{h^3}{12\mu}\frac{\partial p}{\partial\theta}\right)\frac{\partial t}{\partial\theta}-\frac{h^3}{12\mu}\frac{\partial p}{\partial r}\frac{\partial t}{\partial r}\right\}=\frac{\omega^2 r^2\mu}{h}+\frac{\omega h}{2}\frac{\partial p}{\partial\theta} \qquad\qquad (23)$$

$$\rho = A(1-\lambda t) \qquad\qquad (24)$$

$$\mu = B t^{-\beta} \qquad\qquad (25)$$

II.2. Solution of the Governing Equations.

The equations obtained in the previous section are obviously too elaborate to permit an exact mathematical solution. Thus any solution will have to be obtained by numerical means and the method to be used here is the relaxation process introduced by Southwell [11] and applied to lubrication theory by Christopherson [9].

The first step will be to change the independent variables by use of the transformation:

$$\left. \begin{array}{l} \theta = \alpha\,\Theta \\ r = r_o\,e^{\alpha R} \end{array} \right\} \qquad\qquad (26)$$

These equations map the sector shaped pad into a rectangular shaped pad as shown in Figure 1.
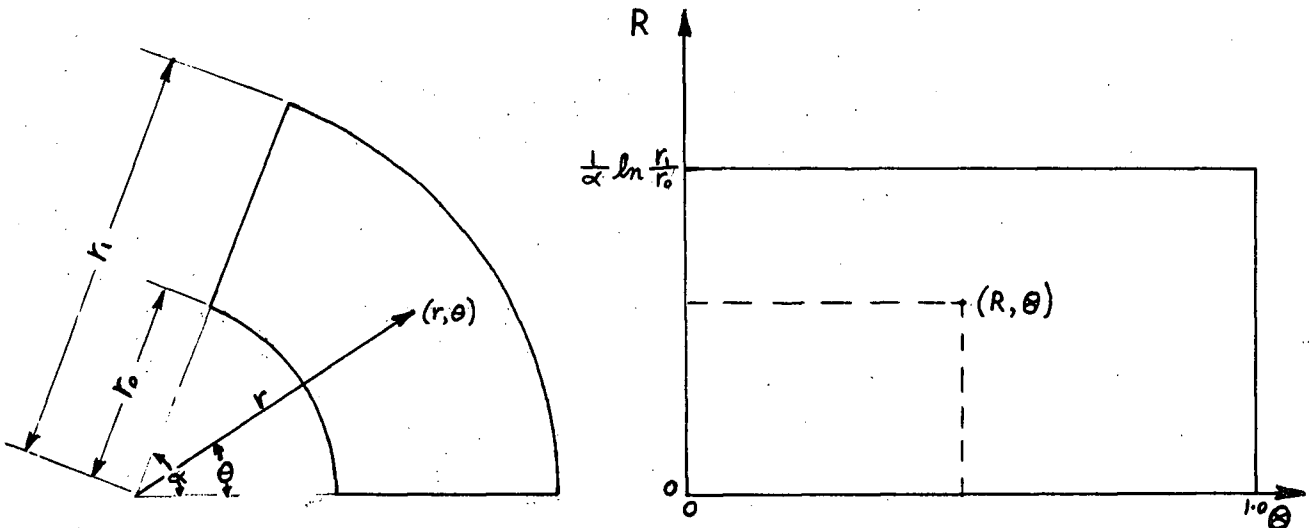
FIG. 1. TRANSFORMATION OF SECTOR INTO RECTANGLE

In terms of the new co-ordinates R and , the governing equations become:

$$\frac{\partial}{\partial\theta}\left(\frac{\rho}{\mu}\frac{\partial p}{\partial\theta}\right) + \frac{\partial}{\partial R}\left(\frac{\rho}{\mu}\frac{\partial p}{\partial R}\right) = \frac{6\alpha\,\omega\,r_o^2}{h^2 e^{-2\alpha R}}\frac{\partial\rho}{\partial\theta} \qquad . \qquad . \quad (27)$$

$$\rho C_p\left\{\left(\frac{\omega h}{2} - \frac{h^3 e^{-2\alpha R}}{12\alpha\mu\,r_o^2}\frac{\partial p}{\partial\theta}\right)\frac{1}{\alpha}\frac{\partial t}{\partial\theta} - \left(\frac{h^3 e^{-2\alpha R}}{12\alpha^2\mu\,r_o^2}\frac{\partial p}{\partial R}\right)\frac{\partial t}{\partial R}\right\} = \frac{\omega^2\mu\,r_o^2}{h\,e^{-2\alpha R}} + \frac{\omega h}{2\alpha}\frac{\partial p}{\partial\theta} \quad . \quad . \quad (28)$$

Next, we render the dependent variables dimensionless by
introducing P, T, D and M which are defind by:

$$
\left.
\begin{aligned}
p &= \frac{6\mu_o\,\omega\alpha\,r_o^2}{h^2}\,P \\
t &= t_o\,T \\
\rho &= \rho_o\,D \\
\mu &= \mu_o\,M
\end{aligned}
\right\} \qquad\qquad . \qquad . \quad (29)
$$

where t_o, ρ_o and μ_o are respectively the temperature, density and viscosity
at the inlet edge. Substitution of equations (29) into equations (24), (25),
(27) and (28) yields:

$$\frac{\partial}{\partial\theta}\left(\frac{D}{M}\frac{\partial P}{\partial\theta}\right) + \frac{\partial}{\partial R}\left(\frac{D}{M}\frac{\partial P}{\partial R}\right) = e^{2\alpha R}\frac{\partial D}{\partial\theta} \qquad . \qquad . \quad (30)$$

$$\left(1 - \frac{e^{-2\alpha R}}{M}\frac{\partial P}{\partial\theta}\right)\frac{\partial T}{\partial\theta} - \left(\frac{e^{-2\alpha R}}{M}\frac{\partial P}{\partial R}\right)\frac{\partial T}{\partial R} = \frac{6\alpha\,\omega\,\mu_o\,r_o^2}{\rho_o C_p h^2 t_o}\frac{1}{D}\left(\frac{M}{3}e^{2\alpha R} + \frac{\partial P}{\partial\theta}\right) \qquad . \quad (31)$$

$$\rho = A\left(1 - \lambda t_o T\right) \qquad\qquad . \qquad . \quad (32)$$

$$\mu = B\left(t_o T\right)^{-\beta} \qquad\qquad . \qquad . \quad (33)$$

It now becomes convenient to call equation (30) the pressure equation,
equation (31) the energy equation, and treat them individually.

Pressure Equation

Making use of the identity:

$$\nabla^2\left(\frac{D}{M}P\right) = P\nabla^2\left(\frac{D}{M}\right) + \frac{D}{M}\nabla^2 P + 2\frac{\partial}{\partial\theta}\left(\frac{D}{M}\right)\frac{\partial P}{\partial\theta} + 2\frac{\partial}{\partial R}\left(\frac{D}{M}\right)\frac{\partial P}{\partial R}$$

in which the operator ∇^2 now stands for $\left(\frac{\partial^2}{\partial\theta^2} + \frac{\partial^2}{\partial R^2}\right)$, the pressure equation
may be written in the form:

$$\nabla^2\left(\frac{D}{M}P\right) - 2\frac{\partial D}{\partial\theta}e^{2\alpha R} = P\nabla^2\left(\frac{D}{M}\right) - \frac{D}{M}\nabla^2 P \quad . \qquad . \quad (34)$$

Christopherson and Southwell [12] have shown that if w is any polynomial

function, the operator ∇^2 could be expressed in finite-difference form by the

equation:

$$a^2 \nabla^2 w = \sum_a w - 4 w_c + \text{terms of order } a^4 \text{ at least,}$$

where the summation sign refers to four points equally spaced on a circle of

radius 'a', whose centre is at the point 'c'.   Substituting this expression

for ∇^2 in the pressure equation gives:

$$\sum_{n=1}^{4} \left[\left(\frac{D}{M} \right)_n + \left(\frac{D}{M} \right)_c \right] P_n - P_c \sum_{n=1}^{4} \left[\left(\frac{D}{M} \right)_n + \left(\frac{D}{M} \right)_c \right] = 2 a^2 \frac{\partial D}{\partial \theta} e^{2 \alpha R} \qquad . \qquad . \qquad (35)$$

where the subscripts now refer to the points on a grid network as shown in

Fig. 2.
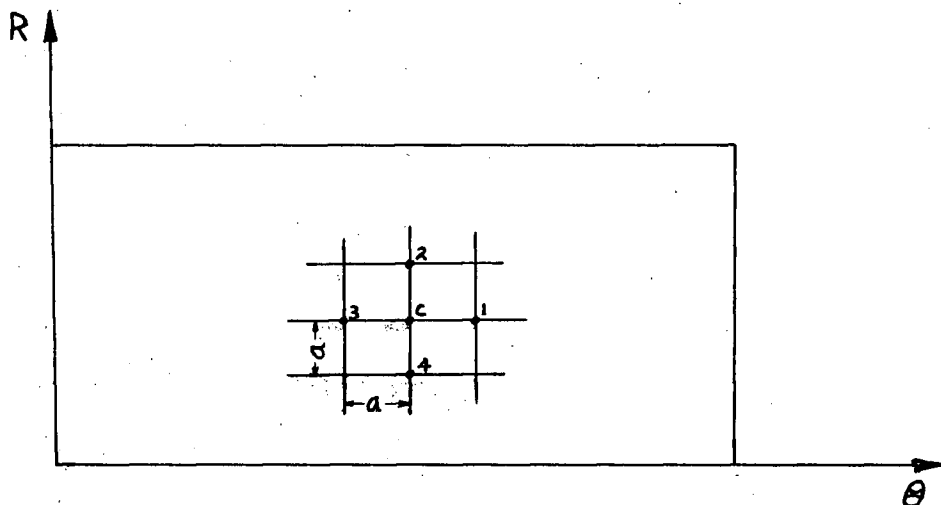
FIG. 2.   GRID POINT NOTATION FOR RELAXATION PROCESS

In the relaxation solution of equation (35), the residual forces and

influence coefficients are defined by:

$$F = \sum_{n=1}^{4} \left[\left(\frac{D}{M} \right)_n + \left(\frac{D}{M} \right)_c \right] P_n - P_c \sum_{n=1}^{4} \left[\left(\frac{D}{M} \right)_n + \left(\frac{D}{M} \right)_c \right] - 2 a^2 \frac{\partial D}{\partial \theta} e^{2 \alpha R} \qquad . \qquad . \qquad (36)$$

$$\left. \begin{aligned} a_{cn} &= \left(\frac{D}{M} \right)_c + \left(\frac{D}{M} \right)_n \\ a_{cc} &= \sum_{n=1}^{4} \left[\left(\frac{D}{M} \right)_n + \left(\frac{D}{M} \right)_c \right] \end{aligned} \right\} \qquad . \qquad . \qquad (37)$$

The effect of any change ΔP on the residual forces is then

$\qquad -a_{cc} \Delta P$ at each point which is altered

$\qquad a_{cn} \Delta P$ at each of the four surrounding points 'n'.

For a given temperature distribution, D and M may be calculated using equations (29). Then, for any assumed distribution of P, the residuals and influence coefficients are calculated from equations (36) and (37). The residuals are now relaxed - that is, the values of P are adjusted in such a way that the residuals are reduced to a negligible value. This procedure gives the pressure distribution corresponding to the given temperature distribution.

Energy Equation

In terms of the grid notation established, the energy equation (31) may be written in finite-difference form to give:

$$\left[1-\frac{e^{-2\alpha R}}{M_c}\left(\frac{P_1-P_3}{2a}\right)\right]\left(\frac{T_1-T_3}{2a}\right)-\left[\frac{e^{-2\alpha R}}{M_c}\left(\frac{P_2-P_4}{2a}\right)\right]\left(\frac{T_2-T_4}{2a}\right)=\frac{6\alpha\,\omega\,\mu_o\,r_o^2}{\rho_o t_o C_p h^2 D_c}\left[\frac{M_c}{3}e^{2\alpha R}+\left(\frac{P_1-P_3}{2a}\right)\right]\quad.\quad(38)$$

For an assumed pressure distribution and a known variation of temperature along the inlet edge of the pad, the corresponding temperature may be obtained throughout the bearing by successive applications of equation (38) across the grid.

Simultaneous Solution for Pressure and Temperature

To summarize, the equations to be solved for the pressure and temperature distributions are:

$$\sum_{h=1}^{4}\left[\left(\frac{D}{M}\right)_h+\left(\frac{D}{M}\right)_c\right]P_h-P_c\sum_{h=1}^{4}\left[\left(\frac{D}{M}\right)_h+\left(\frac{D}{M}\right)_c\right]=2a^2\left(\frac{D_1-D_3}{2a}\right)e^{2\alpha R}\quad.\quad(39)$$

$$\left[1-\frac{e^{-2\alpha R}}{M_c}\left(\frac{P_1-P_3}{2a}\right)\right]\left(\frac{T_1-T_3}{2a}\right)-\left[\frac{e^{-2\alpha R}}{M_c}\left(\frac{P_2-P_4}{2a}\right)\right]\left(\frac{T_2-T_4}{2a}\right)=\frac{6\alpha\,\omega\,\mu_o\,r_o^2}{\rho_o t_o C_p h^2 D_c}\left[\frac{M_c}{3}e^{2\alpha R}+\left(\frac{P_1-P_3}{2a}\right)\right]\quad.\quad(40)$$

$$\rho=A\left(1-\lambda t_o T\right)\qquad\cdot\quad\cdot\quad(41)$$

$$\mu=B\left(t_o T\right)^{-\beta}\qquad\cdot\quad\cdot\quad(42)$$

A simultaneous solution of the above equations may be obtained by first assuming an initial pressure distribution. This pressure distribution enables a first temperature distribution to be obtained using equations (40),

(41) and (42), as described under 'Energy Equation'. This first temperature distribution may then be used to obtain a second pressure distribution from equations (39), (41) and (42), as described under 'Pressure Equation'. The second pressure distribution will lead to a second temperature distribution, and so on. Due to the fact that the viscosity decreases with temperature, the foregoing procedure possesses an inherent stability and the solutions converge after a few iterations.

An IBM 1620 computer has been programmed to perform the foregoing steps and to obtain the solution to equations (39) to (42) in terms of input quantities. These quantities are speed, film thickness and inlet oil temperature.

II.3. Theoretical Performance of Bearing

The test bearing, which will be described in the next chapter, has the limits $0 \leq R \leq 0.5$ and $0 \leq \theta \leq 1$ when it is transformed into a rectangular pad as shown in Figure 1. A grid system was set up on the transformed bearing pad in which the grid dimension 'a' was chosen as 0.1. For this configuration, a total of 66 points existed which were to describe the pressure and temperature distributions corresponding to equations (39) to (42).

For an arbitrarily chosen initial pressure distribution, the corresponding temperature field was calculated. A revised pressure distribution was then obtained by relaxing the pressure residuals in 7 discrete stages of up to 15 passes per stage as required. At this point the residuals were reduced to about 0.1% of their initial value. Successive solutions were carried out for a total of 3 iterations. No modification to the pressure and temperature distributions were noticed when more than 3 iterations were performed, consequently the values obtained after 3 iterations were accepted as simultaneously satisfying equations (39) to (42).

The quantities to be established from the pressure and temperature distributions are the load carrying capacity of the bearing and the corresponding coefficient of friction.

Load Carrying Capacity

For the derived pressure distribution, the load carried per pad was obtained by integration. That is,

$$W = \int_{r_0}^{r_1} \int_0^\alpha p\, r\, dr\, d\theta \qquad (43)$$

The above integration was incorporated in the computer program so that the load carried per pad was obtained directly for each pressure distribution.

For safe operation of the bearing, the pressure distribution should be limited such that:

(i) the maximum temperature does not exceed 220°F and

(ii) the film thickness is not less than 0.0002 inch.

The first criterion is intended to ensure that the babbit does not melt whilst the second should ensure the absence of metal to metal contact. The bearing load corresponding to the smallest limiting pressure distribution was considered to be the load carrying capacity of the thrust pad.

Coefficient of Friction

Considering the friction force on a fluid element to be due to the shearing action across the film, we may write:

$$dF_f = \tau_{z\theta}\, r\, dr\, d\theta$$

$$i.e. \quad dF_f = -\mu \frac{\partial v_\theta}{\partial z}\, r\, dr\, d\theta$$

where the expression for $\tau_{z\theta}$ has been substituted from equations (8) with v_z set equal to zero. The expression for   is given in equations (19) and may be substituted to give:

$$dF_f = \left[\frac{1}{2}\frac{\partial p}{\partial \theta}(h - 2z) + \frac{\mu \omega r^2}{h}\right] dr\, d\theta$$

for any point in the fluid film. In particular, at $z=0$ we get:

$$dF_f = \left(\frac{h}{2}\frac{\partial p}{\partial \theta} + \frac{\mu \omega r^2}{h}\right) dr\, d\theta$$

so that the total friction force per pad is given by:

$$F_f = \int_{r_0}^{r_1} \int_0^\alpha \left(\frac{h}{2}\frac{\partial p}{\partial \theta} + \frac{\mu \omega r^2}{h}\right) dr\, d\theta$$

Integrating the first term in this expression with respect to θ and noticing that $p=0$ at $\theta=\alpha$ and $\theta=0$:

$$F_f = \int_{r_0}^{r_1} \int_0^\alpha \frac{\mu \omega r^2}{h}\, dr\, d\theta$$

The coefficient of friction is defined as the ratio of the transverse friction force to the applied bearing load.

That is,

$$f = \frac{F_f}{W}$$

$$i.e. \quad f = \int_{r_o}^{r_i} \int_o^\alpha \frac{\mu \omega r^2}{W h} \, dr \, d\theta \qquad \qquad (44)$$

Equation (44) was also incorporated in the computer program.

Bearing Performance Curves

Using equations (39) to (44), the load carrying capacity and the coefficient of friction for the test bearing were obtained at speeds of 15,000 and 20,000 r.p.m. The results are shown graphically in Figures 3 and 4. In calculating these results, the inlet oil was assumed to be at a temperature of $70°F$ and the physical properties of the lubricant as given in Appendix II were used. The load carrying capacity is seen to be 40 lbs. at both speeds. In fact, for any selected limiting temperature, the load carrying capacity is seen to be the same. The only difference between the limiting conditions is the film thickness at which the limiting load is carried. This fact can be understood by considering the action of the thermal wedge. The load carried depends on the temperature rise across the bearing and hence the density change. The necessary temperature rise may be achieved at low speed with thin fluid films or at high speed with greater film thicknesses. However, the high speed condition has the advantage of having a lower coefficient of friction.

FIG. 3 THEORETICAL PERFORMANCE AT 15,000 r.p.m.
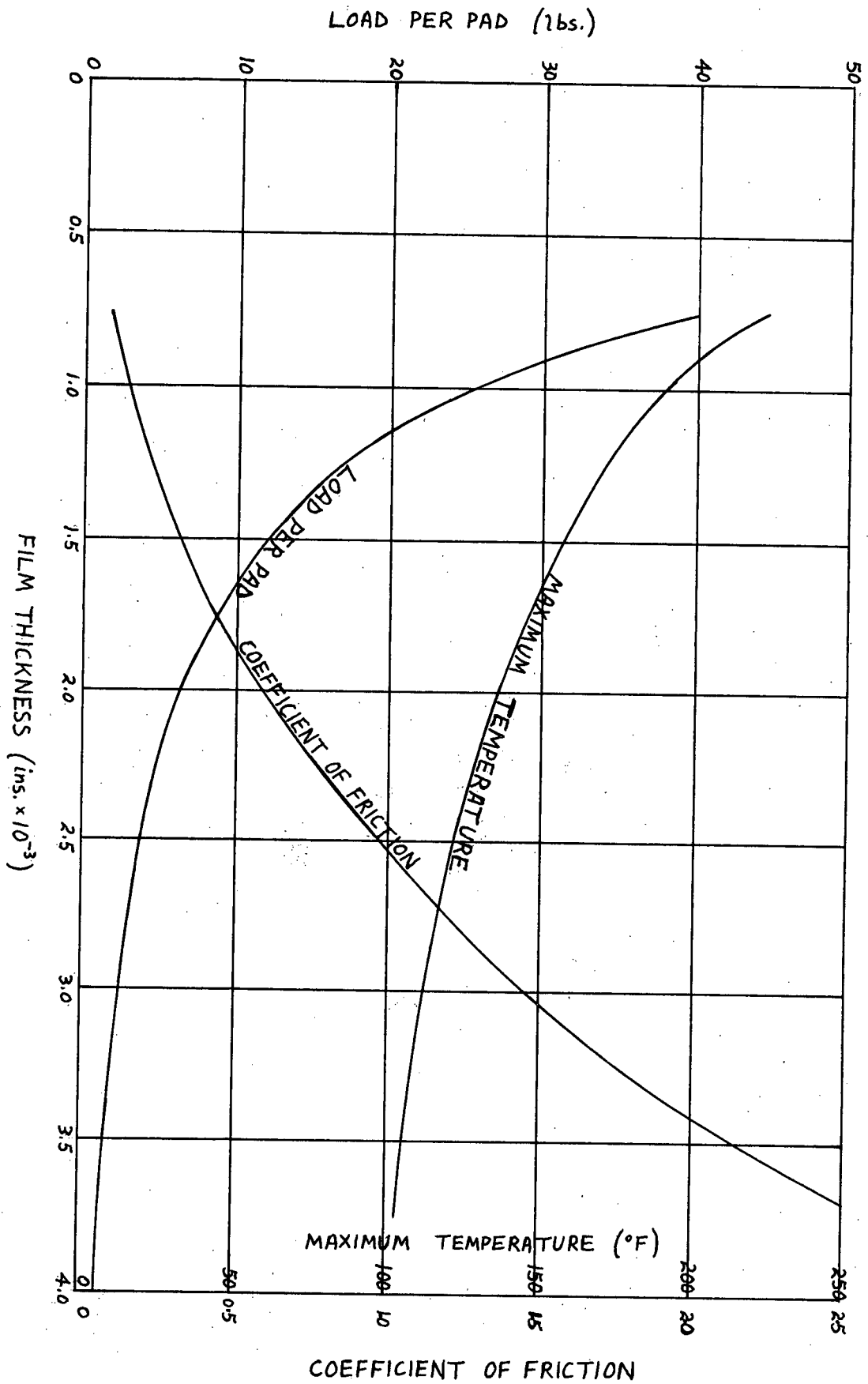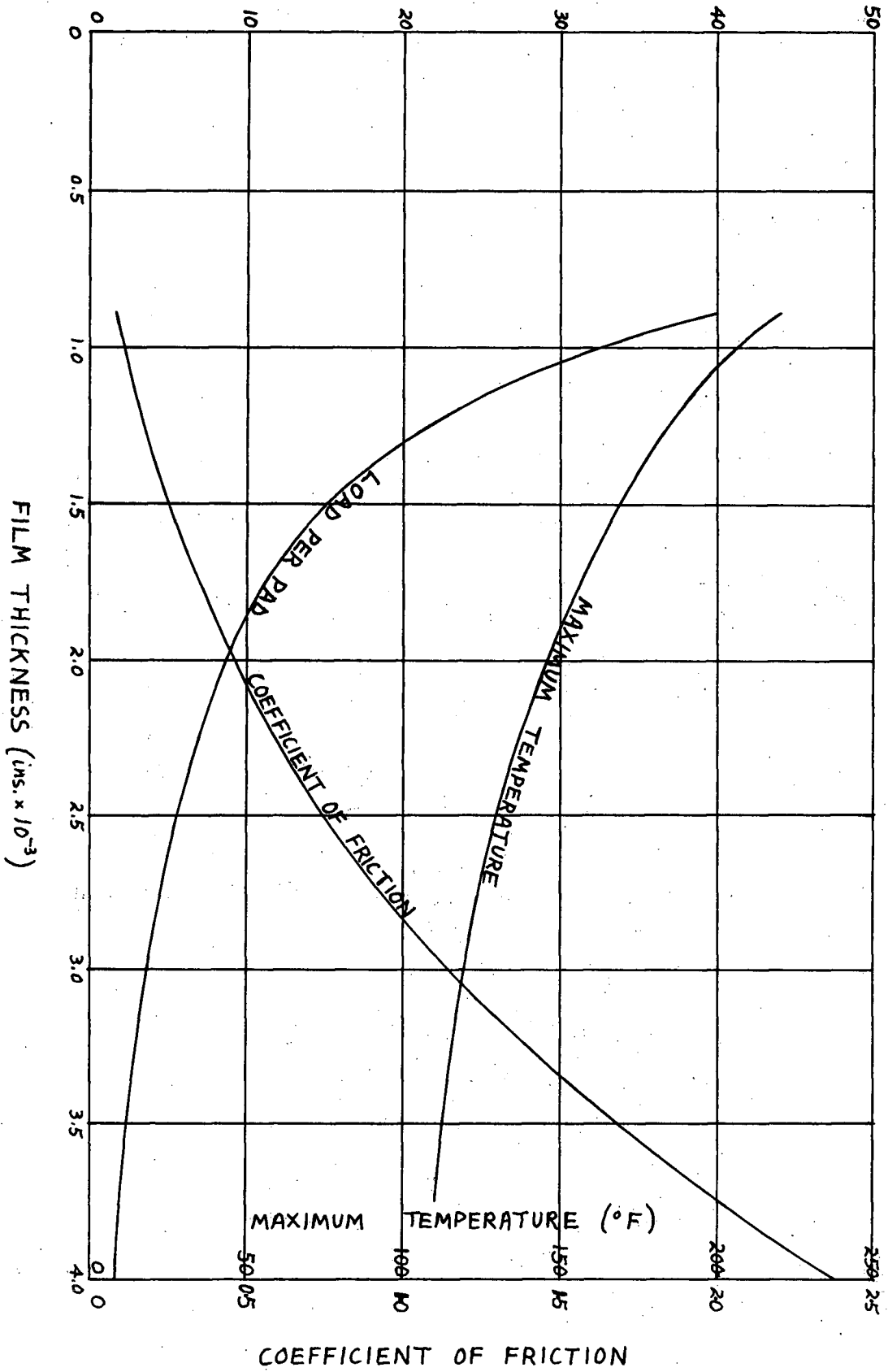
FIG. 4 THEORETICAL PERFORMANCE AT 20,000 r.p.m.

CHAPTER III

III. 1. Apparatus and Measurements

III.1. Apparatus and Measurements

(i) Apparatus

The schematic layout of the apparatus is shown in Figure 5. The drive system consisted of an electric motor, a V-belt drive and a gear box. The 15 h.p. induction motor ran at 3,545 r.p.m. under full load. The V-belt drive consisted of one 4.0/5.4 inch vari-pitch pulley, which was fitted to the motor shaft, and one of three interchangeable fixed-pitch pulleys of 7.0, 9.0 and 12.4 inch diameters, which could be fitted to the intermediate shaft. The intermediate shaft was direct coupled to a Rolls-Royce Merlin supercharger gear box which had a 9.5:1 step up ratio. With this drive system the test bearing could be run at almost any speed from 11,000 to 26,000 r.p.m.

A sectional view of the test bearing assembly is shown in Figure 6. The high speed shaft consisted of a $\frac{5}{8}$ inch diameter steel rod on which a 3 inch diamter steel disc had been shrunk. The opposing faces of the thrust disc were machined, and subsequently lapped, so that they were flat and parallel to within 1.0×10^{-4} inch and had a surface finish of about 12 microinches. The high speed shaft was supported by two double row, self aligning, ball-type bearings which were lubricated by an oil drip system. The critical speed of the high speed shaft assembly was about 10,000 r.p.m.

A steel cylinder concentric with the high speed shaft surrounded the thrust disc. This cylinder carried three matched hydraulic jacks which operated in parallel and were located at 120° to each other around the outside of the cylinder. The jacks were connected to two triangular end plates which were in contact with the two opposing loading pistons in the steel cylinder. The loading pistons carried two similar babbitted thrust collars, as shown in Figure 7, which formed bearing surfaces for the faces of the thrust disc.

The complete cylinder assembly was torque mounted and supported by two steel piston tubes which were attached to the loading pistons and which were concentric with the high speed shaft. The piston tubes were supported at their outer ends by two roller bearings as shown in Figure 8.

The roller bearing housings were used to admit oil to the test surfaces. Seals were provided between the bearing housing and the high speed shaft, and between the housing and the piston tube. The lubricant flowed in the annular space between the piston tube and the high speed shaft and into the space between the bearing surfaces. The assembled bearing is shown in its test position in Figure 9.

Oil was supplied from a 45 gallon tank, which was located about 11 feet above the test bearing, and the outlet oil was gravity fed to another 45 gallon tank which was located about 4 feet below the bearing. A motor and pump unit returned the oil to the upper tank at the end of each test. The oil used was Shell Turbo 27; the physical properties of this oil are given in Appendix II.

A separate oil system supplied lubricant to the gear box. Oil from a reservoir was pressure fed to the gear box by means of a gear pump. Another pump drained the gear box sump and returned the oil to the reservoir. Both pumps were driven from the same electric motor.

(ii) Measurements

The essential quantities to be measured under test were speed, load, torque, temperature and film thickness.

Speed

The rotational speed of the high speed shaft was measured directly by use of a 'Smith's' tachometer which had speed ranges from 0-5,000 and 0-50,000 r.p.m. The instrument had a resolution of 0.4% of the full

scale.

Load

The bearing load was assessed by measuring the pressure applied to the loading jacks. The pressure was obtained from an 'American' pressure gauge tester which was capable of supplying pressures of up to 500 lbs./sq.in. in increments of 5 lbs./sq.in. The calibration curve for the loading system is given in Appendix III.

Torque

The friction torque transmitted to the thrust pads was measured by means of a weight pan which was knife-edge suspended on a torque arm. The torque arm was mounted on the bearing torque ring and weight pan was situated at a distance of 10 inches from the bearing centerline.

Temperature

The temperature of the oil was measured at the inlet and outlet of each sector of the thrust pad at the points shown in Figure 7. Two thermocouples were placed in each oil groove. The thermocouples were mounted in tufnol inserts which were screwed into the brass backing plate of the thrust pad. Thermocouple potential was measured by a 'Doran'thermocouple potentiometer which had ranges of 0.20mV, by increments of 0.01 mV, and 0-100 mV by increments of 0.05 mV. This instrument is shown in Figure 10. Copper-constantan thermocouples were used and the calibration procedure and results are given in Appendix III.

Film Thickness

The thickness of the fluid film in the bearing was measured by means of a 'Daytronic' model 103A-80 linear displacement transducer, which is shown in Figure 11. This transducer had a range of 0.040 inch and was fitted with a special steel tip which had a hemispherical end of radius 0.030 inch. The transducer was screwed into the loading piston crown, as shown in

Figure 5, and the plunger tip passed through the thrust pad to make contact with the thrust disc. Thus the electrical output of the transducer was a measure of the distance between the thrust pad and the thrust disc.

A 'Daytronic' model 300BF differential transformer indicator supplied the excitation for the transducer and showed the displacement on a pre-calibrated scale. This instrument, which is shown in Figure 10, had a range of $\pm$ 0.100 inch and a maximum resolution of 10 microinches.

In addition to the transducer, two 'Starrett' $\frac{1}{10,000}$ inch dial gauges were mounted on the steel cylinder with their plungers touching one of the piston end plates. The configuration was such that the gauges recorded the sum of the two film thicknesses.

The aforementioned instruments and pieces of equipment are shown in their test positions in Figure 12.
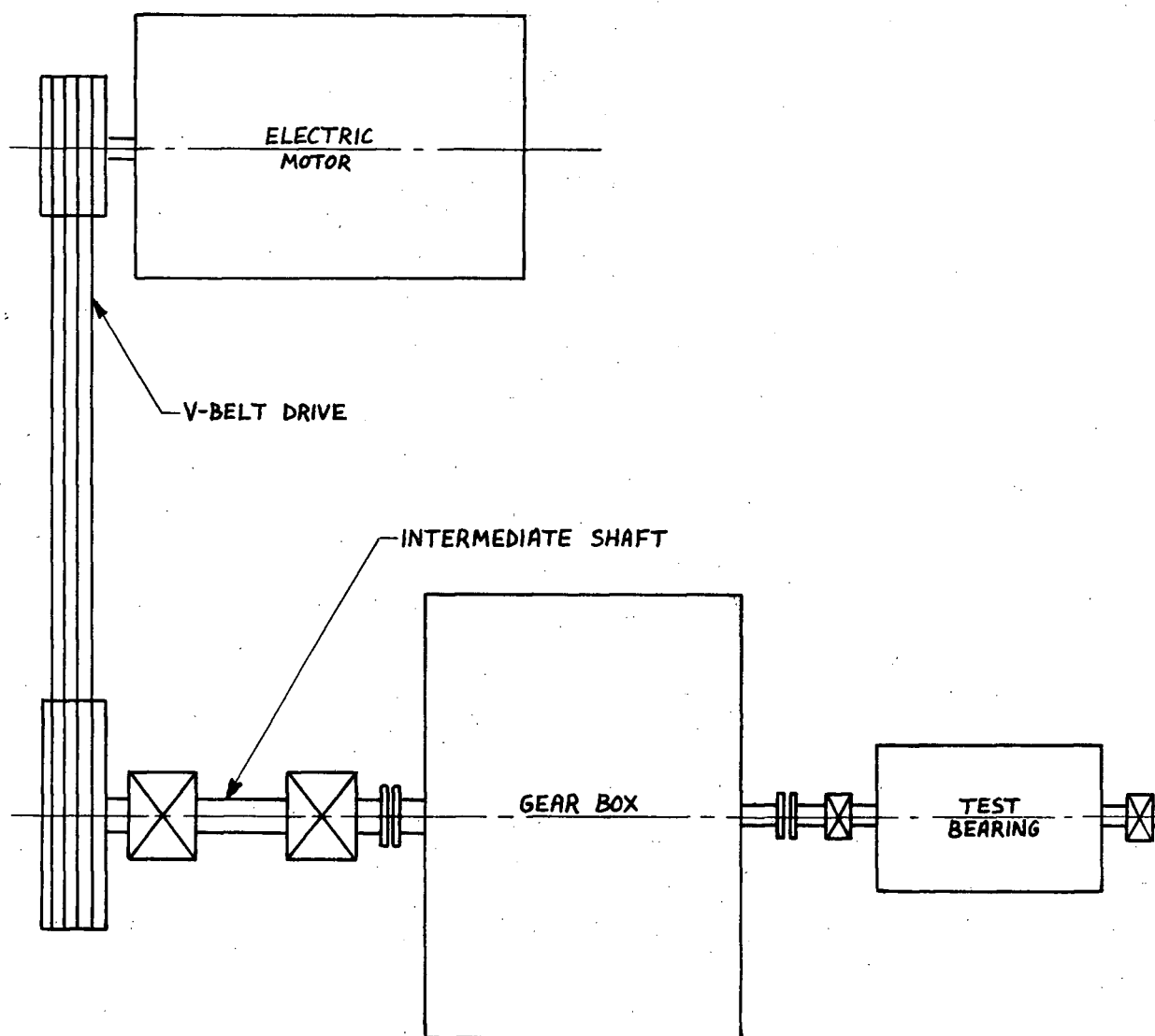
FIG. 5 SCHEMATIC LAYOUT OF APPARATUS
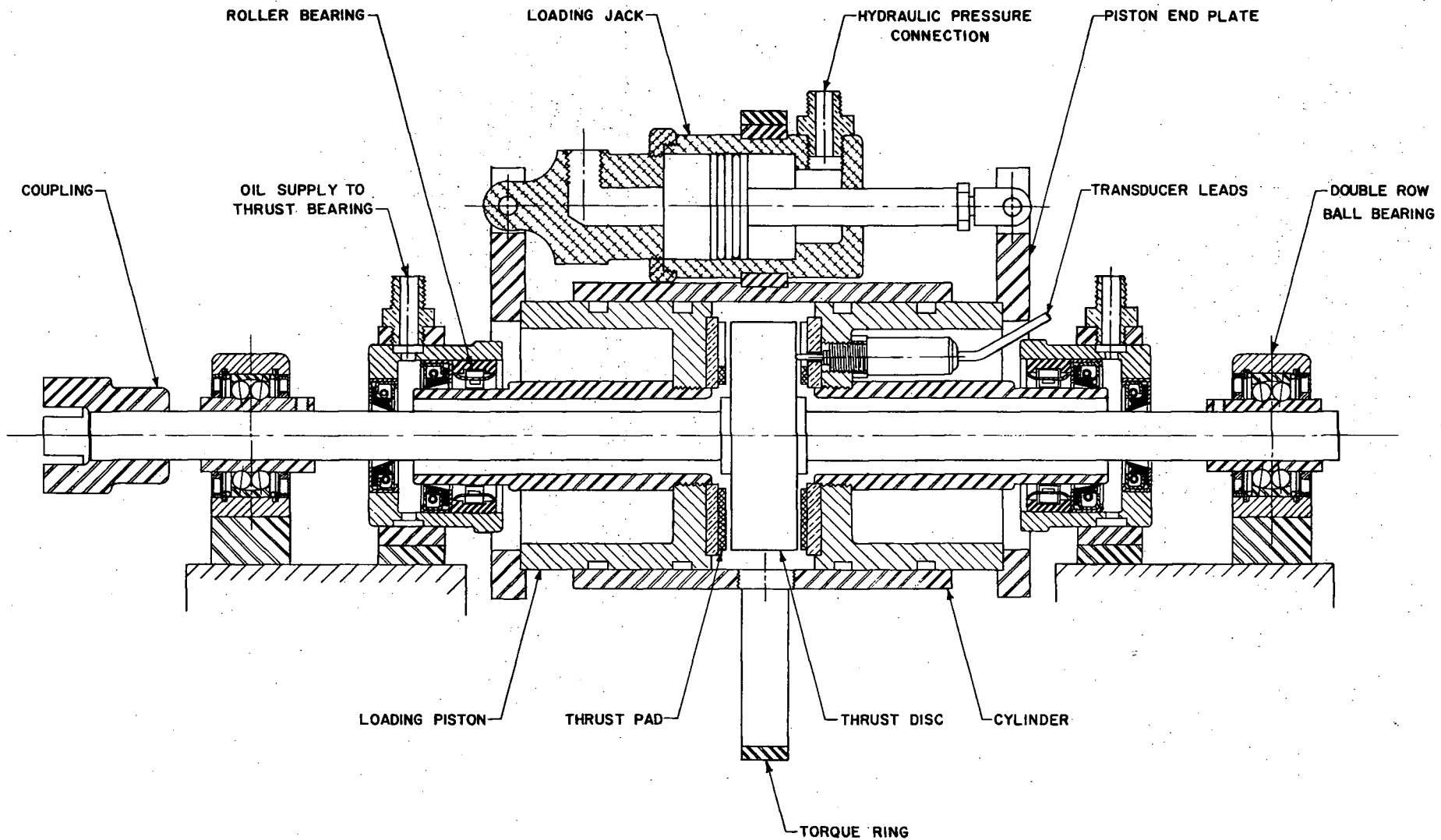
FIG. 6 SECTIONAL VIEW OF TEST BEARING
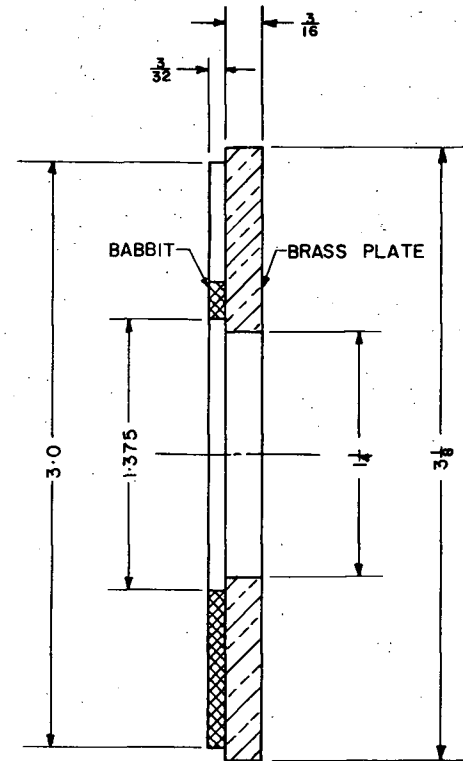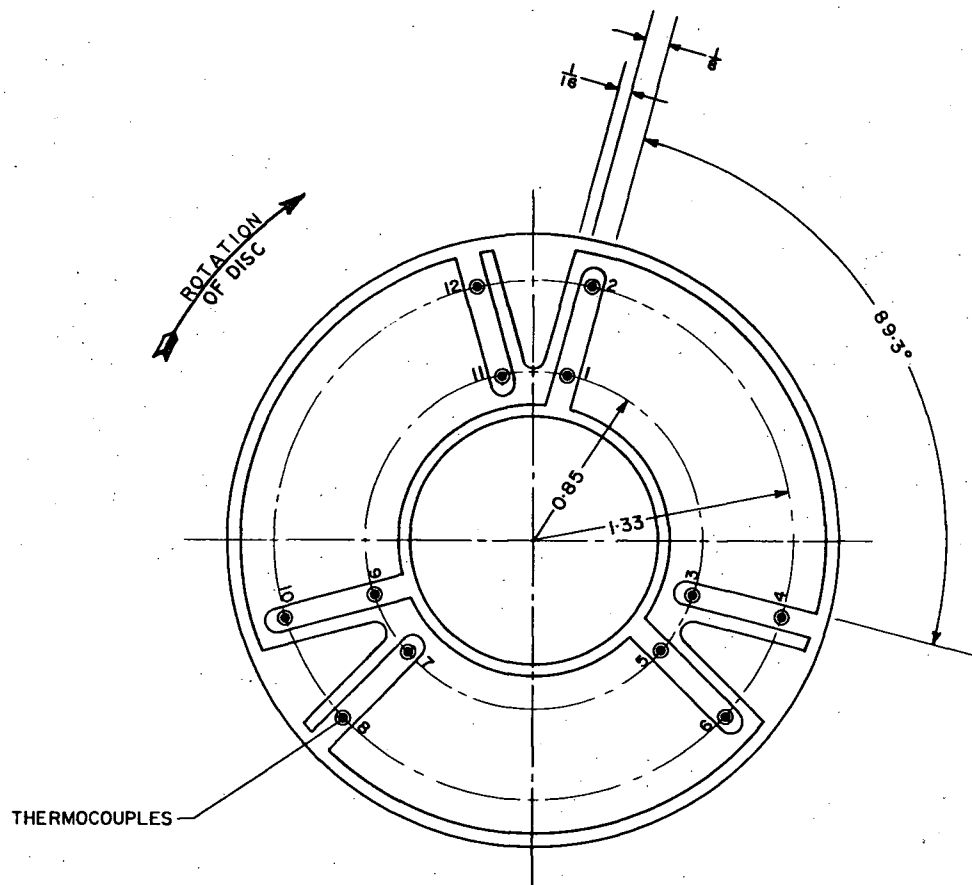
FIG. 7 DETAILS OF THRUST PAD
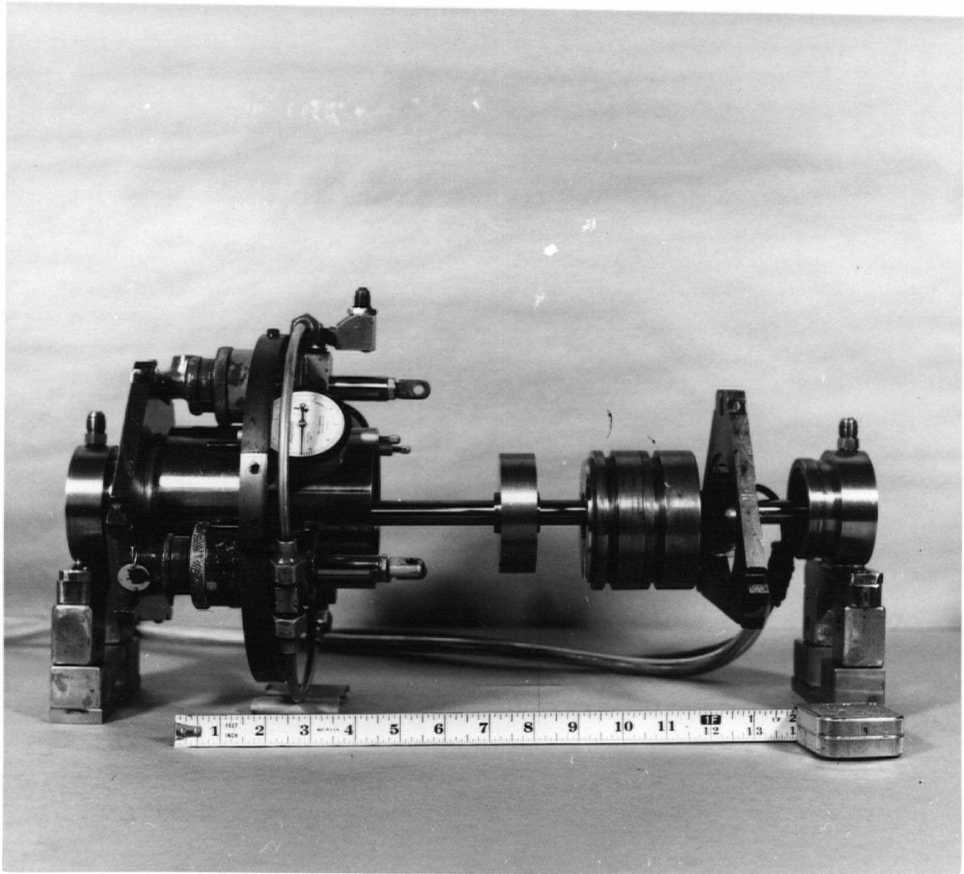
FIG.8   TEST BEARING BEFORE ASSEMBLY
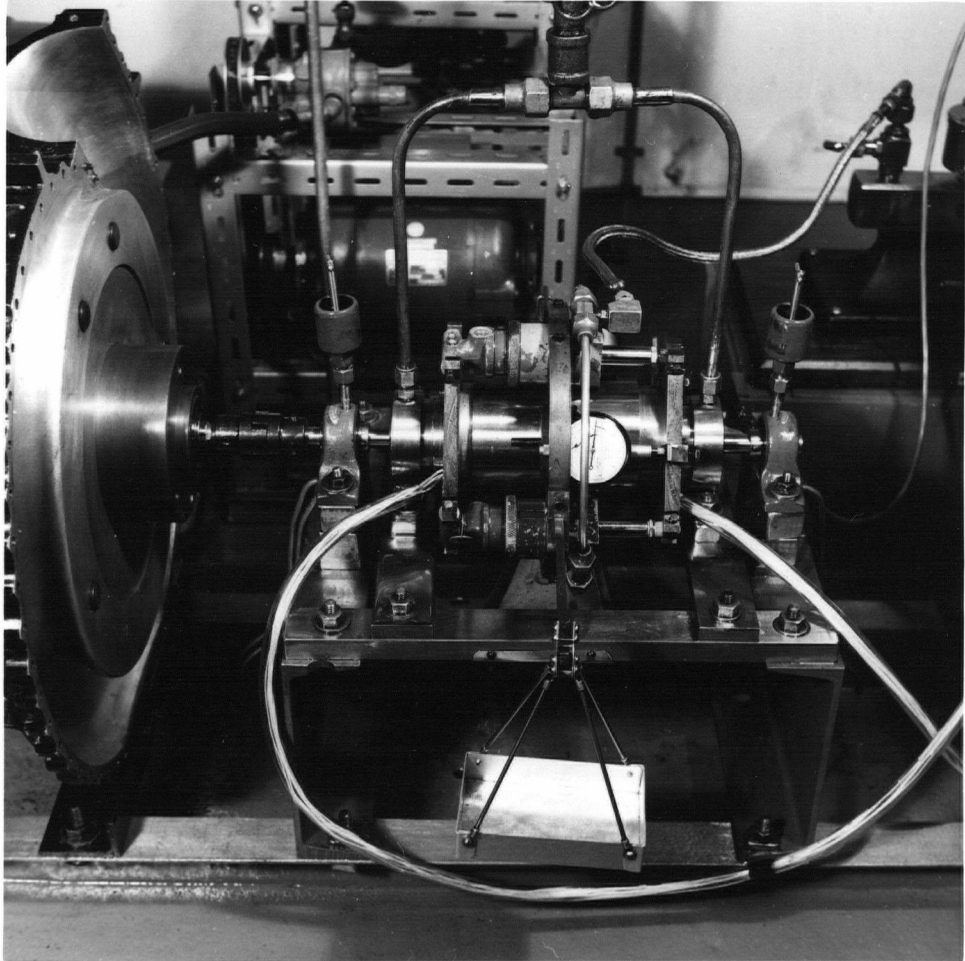
FIG.9   ASSEMBLED BEARING IN POSITION
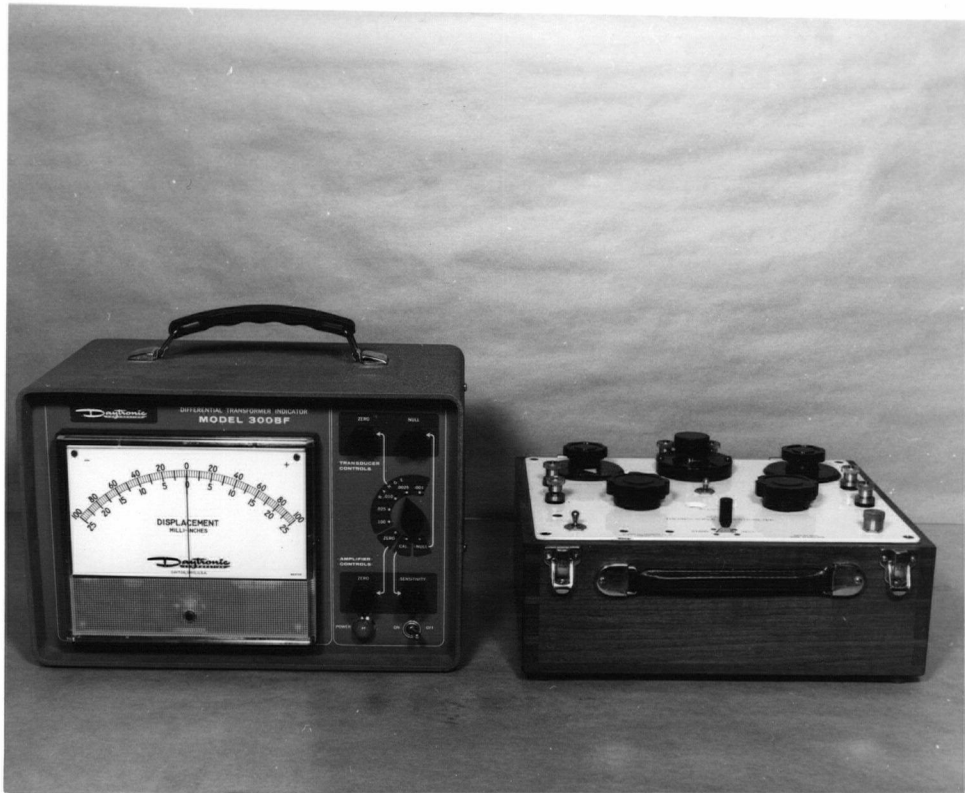
FIG.10   DIFFERENTIAL TRANSFORMER INDICATOR AND THERMOCOUPLE

POTENTIOMETER
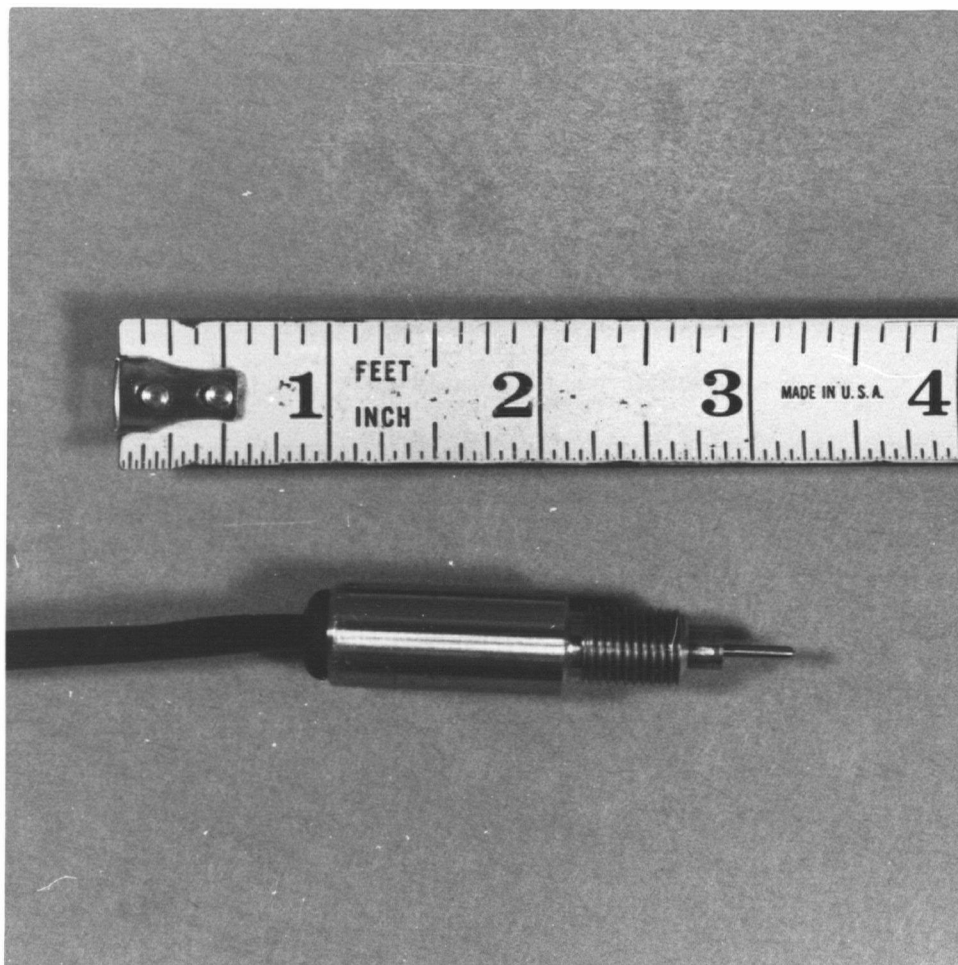
FIG.11   DISPLACEMENT TRANSDUCER WITH SPECIAL TIP
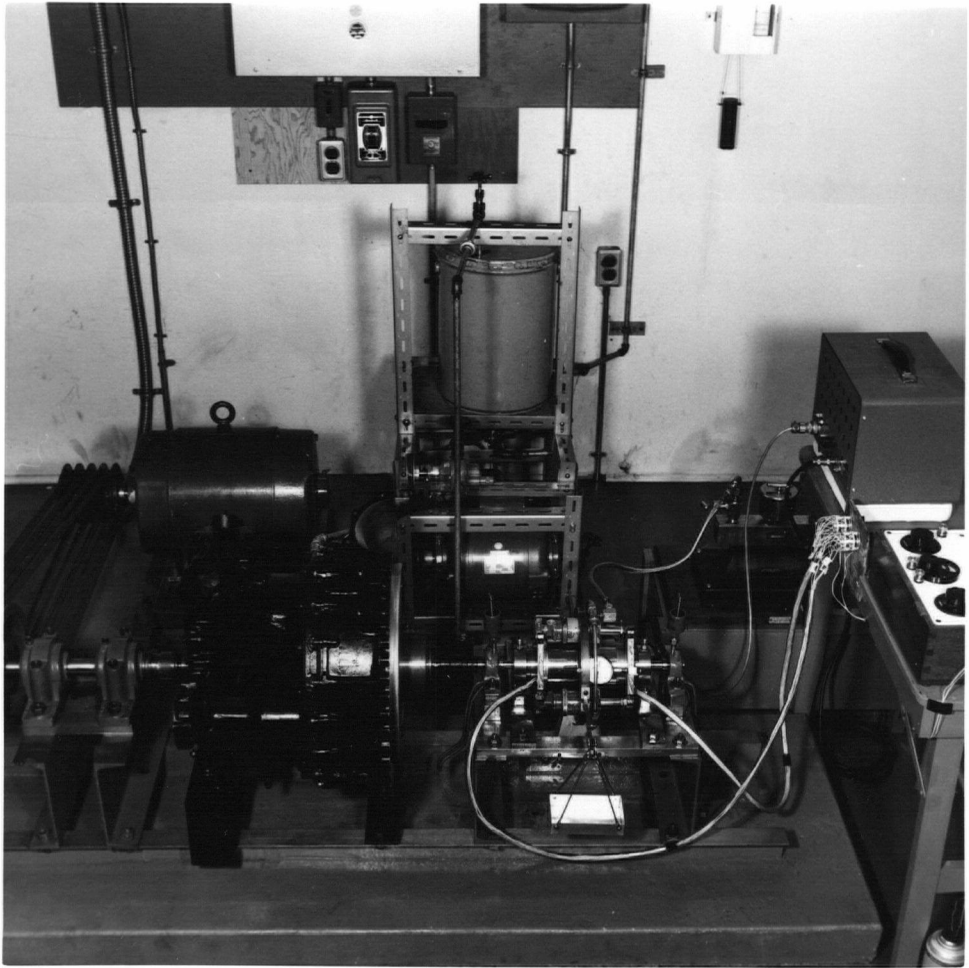
FIG.12 GENERAL VIEW OF APPARATUS

CHAPTER IV

IV.1. Experimental Procedure

A particular assembly procedure for the test bearing was adopted to ensure proper alignment of the thrust surfaces prior to a series of tests. With the entire bearing assembled but unbolted, the high speed shaft was secured by bolting down the two support bearings. With the normally stationary parts of the test bearing assembly still unsecured, a load was applied to the thrust surfaces, so causing metal to metal contact between the thrust pads and the thrust disc. The resulting contact pressure caused the test bearing assembly to align itself with the thrust disc. With the load still applied to the bearing, the two roller bearings which support the stationary components were carefully secured.

Before beginning each test, a pressure of 25 lbs./sq.in. was applied to the loading jacks to bring the thrust surfaces into contact and the differential transformer indicator and dial gauges were set to read zero. The load was then removed from the bearing and the thrust surfaces were separated by about 0.010 inch. The stationary components were torque balanced in this position.

With these preliminaries completed, the lubrication system for the gear box was started and oil was admitted to the test surfaces. The main motor was then started and an initial loading pressure of 5 lbs./sq.in. was applied to the hydraulic loading jacks. After about two minutes running time the oil temperature in the bearing stabilized and test readings could be taken. Readings of speed, torque, film thickness and oil temperature were recorded. The rate of oil flow through the bearing and the bulk outlet temperature of the oil were recorded as supplementary information.

The foregoing procedure was repeated for loading pressure increments of 5 lbs./sq.in. until the outlet oil temperature was about $220°$ F. The maximum temperature criterion, rather than the minimum film thickness

criterion, was found to limit the load carrying capacity of the bearing.   At this point the bearing was unloaded and the machine was stopped.   Immediately the machine was at rest, a loading pressure of 25 lbs./sq.in. was quicly applied to the loading jacks and the transducer zero reading noted while the bearing components were still hot.   The load was then removed and the thrust surfaces were separated by about 0.010 inch and the zero torque reading was checked.

The test procedure was repeated for speeds ranging from 15,000 to 19,000 r.p.m.   Tests at speeds in excess of 19,000 r.p.m. could not be made due to the persistent cage failure of a roller bearing in the high speed end of the gear box.

Having completed a series of tests, the test bearing was dismantled for inspection.   The thrust surfaces were found to be in good condition with no evidence of metal to metal contact under running conditions. The bearing was reassembled and the previous tests repeated;   the results obtained were found to be in agreement with the first set of readings.

IV.2. Experimental Results

The derived results are presented in graphical form in this section and the observed results are given in Appendix IV. The load curves for the bearing are shown in Figure 13 and the corresponding friction characteristics are shown in Figure 14. To permit a direct comparison to be made with the theoretical curves obtained in Chapter II, the curves for 20,000 r.p.m. have been reproduced in Figures 13 and 14. The theoretical curves for a speed of 15,000 r.p.m. lie very close to those for 20,000 r.p.m., consequently the former curves have been omitted. Experimentally, it was found that loads in excess of 16.5 lbs. per pad could not be carried by the bearing without the outlet oil temperature exceeding the specified limit of $220°F$.

The experimental results obtained may be compared with the results obtained by other investigators by plotting the coefficient of friction f against the parameter $\frac{ZN}{P'}$. Such a plot is shown in Figure 15 in which the value of Z has been taken in centipoise, N is in r.p.m. and P' is in lbs./sq.in.

To obtain the coefficient of friction from the measured bearing torque and load, a mean radius of the bearing must be defined. The theoretical expression for the coefficient of friction is given by equation (44):

$$f = \int_{r_o}^{r_1} \int_{o}^{\alpha} \frac{\mu \omega r^2}{W h} \, dr \, d\theta$$

If the viscosity is assumed constant at some average value μ', then the above equation may be integrated to give:

$$f = \frac{\mu' \omega \alpha}{W h} \left(\frac{r_1^3 - r_o^3}{3} \right) \qquad \qquad . \qquad . \quad (45)$$

For an applied load of P' per unit area, the load per pad W will be given by the expression:

$$W = P' \alpha \left(\frac{r_1^2 - r_o^2}{2} \right)$$

Substituting for W in equation (45) yields:

$$f = \frac{\mu' \omega}{P' h} \frac{2}{3} \left(\frac{r_i^3 - r_o^3}{r_i^2 - r_o^2} \right) \qquad \cdot \qquad \cdot \qquad (46)$$

From equation (46), the mean bearing radius r_m is defined by:

$$r_m = \frac{2}{3} \left(\frac{r_i^3 - r_o^3}{r_i^2 - r_o^2} \right) \qquad \cdot \qquad \cdot \qquad (47)$$

For the bearing tested, $r_i = 1.5$ and $r_o = 0.6875$ so that $r_m = 1.144$ inches. Having defined the mean radius of the bearing, the experimental coefficient of friction may be obtained from the measured friction torque per pad by using the relation:

$$f = \frac{T_f}{W r_m} \qquad \cdot \qquad \cdot \qquad (48)$$
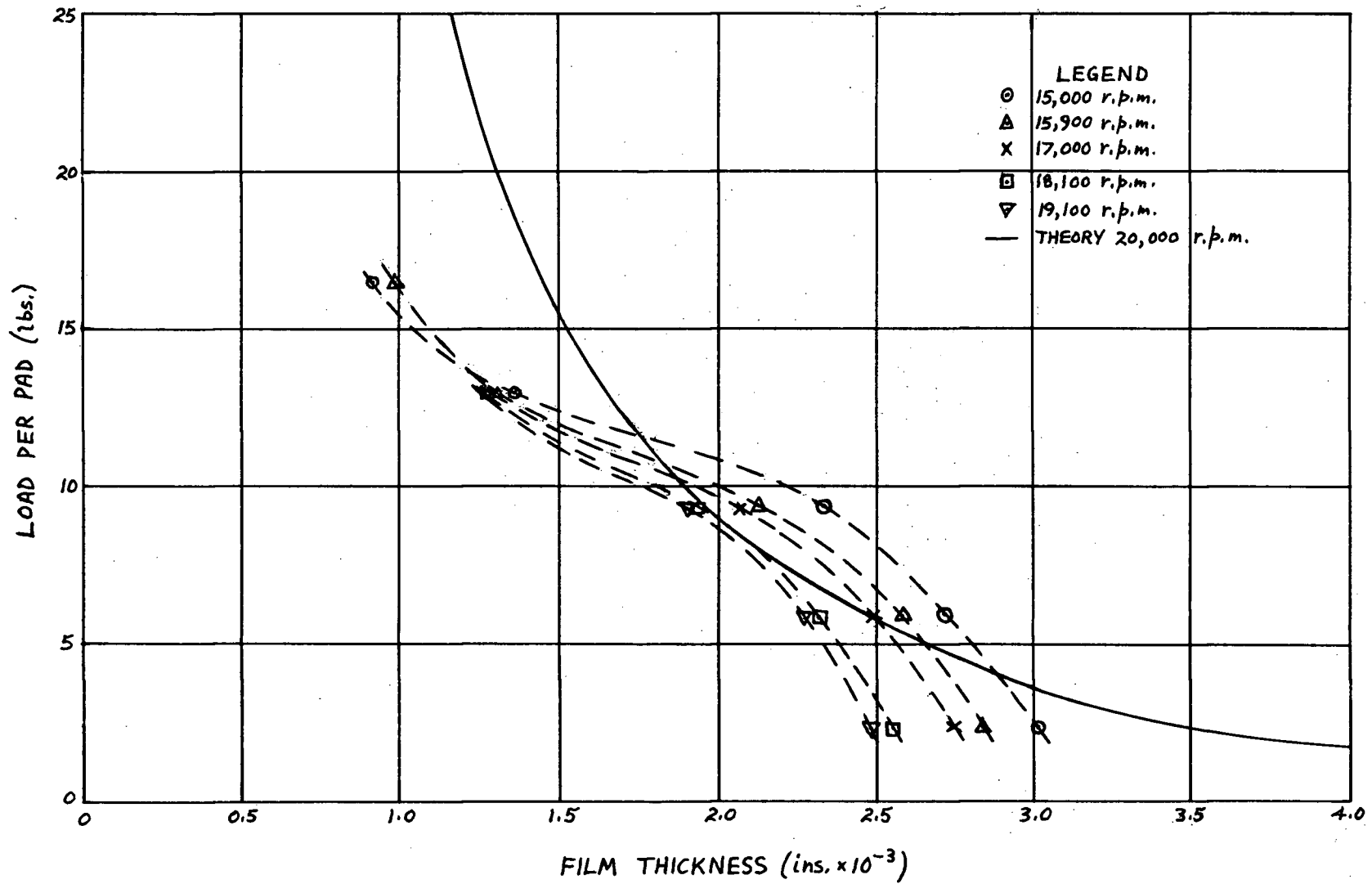
FIG. 13 EXPERIMENTAL LOAD CARRYING CAPACITY
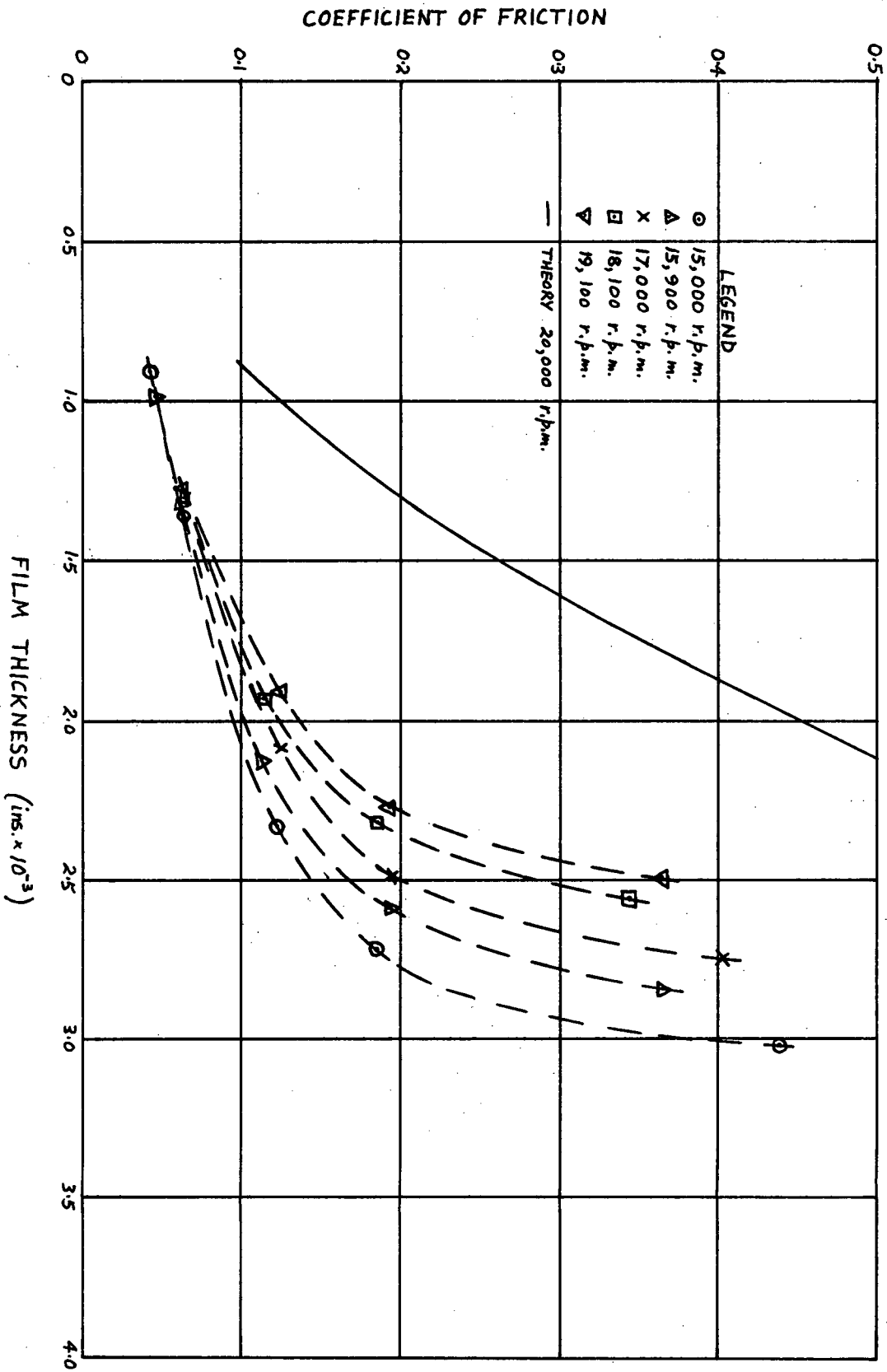
FIG. 14 EXPERIMENTAL COEFFICIENT OF FRICTION
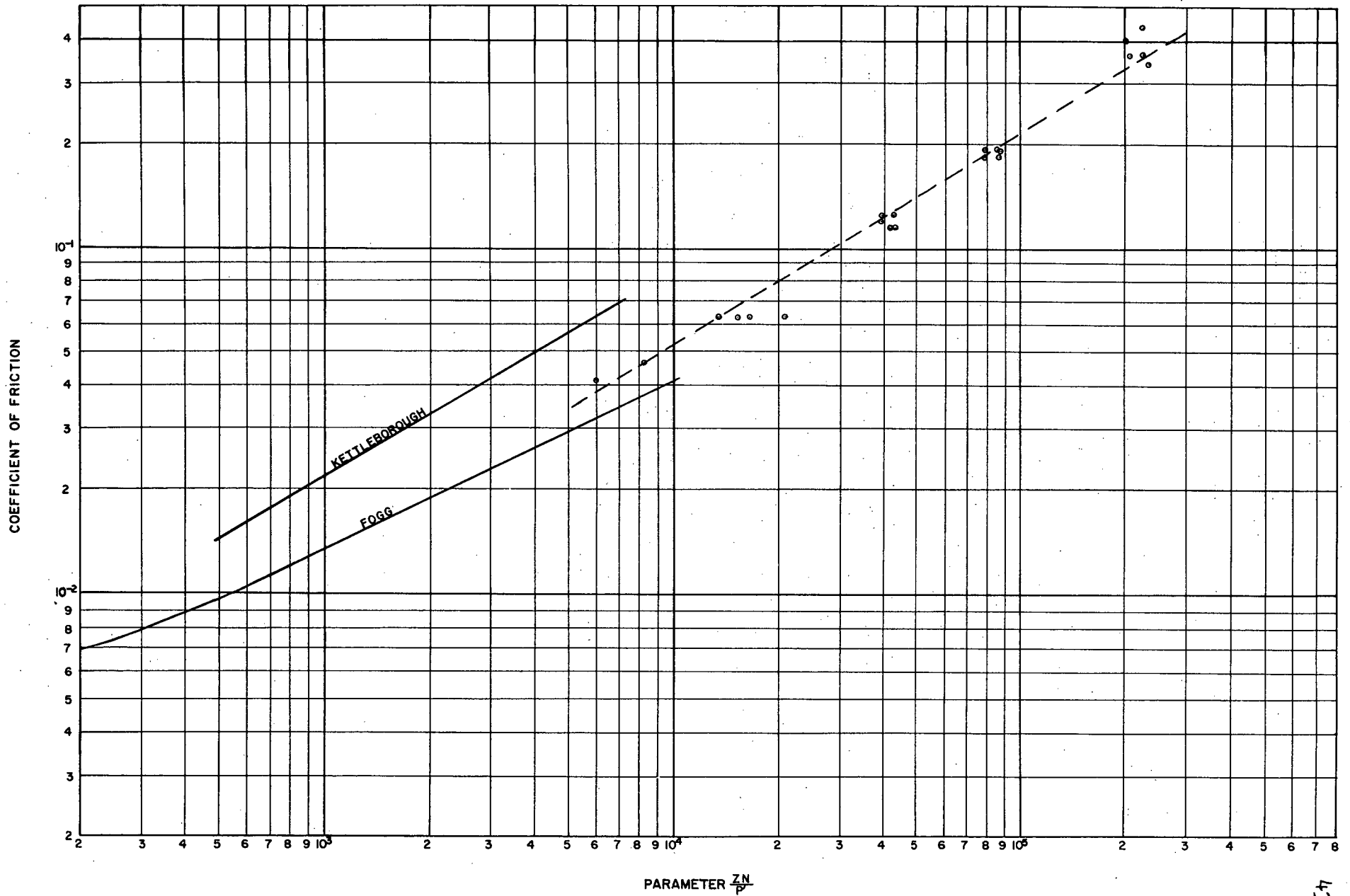
FIG. 15 COMPARISON OF EXPERIMENTAL DATA

IV.3. Discussion of Results

        An estimate of the accuracy of the observed results will be made, together with some general comments. This discussion will be followed by a comparison of the experimental results with the theoretical predictions. Finally, the experimental results will be compared with those obtained by other investigators.

Observed Results

        For each nominal speed setting, the rotational speed of the thrust disc was found to be independent of the applied bearing load. The accuracy of the speed meansurements was limited only by the readability and inherent accuracy of the tachometer. For the speeds at which the bearing was run, the recorded figures may be considered as being accurate to within 0.2%.

        The accuracy with which the bearing load was obtained was governed by the accuracy of the calibration curve for the loading system. In Appendix III the loading curve is given to within 5%.

        The friction torque, as measured, was produced by the action of both thrust bearings. The balancing system was found to be sensitive to within ½ an ounce or about 5%. The probable accuracy of the coefficient of friction, if based on the root mean square law, is 7%.

        The accuracy of the film thickness recordings was governed by the random deviations which were experienced. Suppose that the film thickness was nominally 0.0010 inch. It was found that this value would prevail for 1 to 2 seconds, then it would falter briefly to about 0.0009 inch and return to 0.0010 inch after a small overshoot. This erratic deviation limited the accuracy of the film thickness measurements to about 10%.

        Accompanying the variation in film thickness, a variation in the temperature of the outlet oil was observed. It was noticed that if the

film thickness decreased, the oil temperature increased, the variations in temperature being of the same nature and duration as the variations in film thickness. The accuracy of the temperature measurements were consequently limited to be within an estimated figure of 5% of the recorded values.

From the foregoing description of the variations in film thickness and temperature, it was thought that intermittent oil starvation existed between the bearing surfaces. Evidence of localised oil starvation was also reported by Fogg [2]. To ensure that the thrust pads were operating fully flooded, Fogg fitted circumferential oil seals to his test bearing. The resulting restriction to oil flow at the perimeter of the bearing produced a small positive pressure there and a considerable improvement in the bearing capacity was obtained.

Another factor which could contribute to the instability exhibited by the test bearing is the presence of air between the thrust surfaces. Air entering the bearing, either by way of the inlet oil or through the outlet grooves, would create a region which would move across the bearing and which would support little or no load.

The observed results show that the temperature in the inlet oil grooves rose to very high values even although the supply oil was at 70°F. The high temperatures recorded would appear to be caused by leakage of the outlet oil from one pad into the inlet of the next pad. This leakage could take place by either one of two mechanisms.

The first mode of leakage could be attributed to carry-over from the rotating disc. That is, since there exists a definite gap between the stationary and moving surfaces of the bearing, and since the layer of oil next to the disc is moving with the disc, it is evident that some recirculation will always take place. By this means it may be visualized that the fluid film at the inlet to a pad will be made up of entirely recirculated oil in

the layer adjacent to the disc, entirely fresh oil adjacent to the stationary pad, and some form of mixture in the region between these extreme layers.

The second method by which oil may leak from one pad to another is related to the particular thrust pad configuration employed. Referring to Figure 7, it will be seen that oil entering the outlet groove containing thermocouples 11 and 12 will be unable to escape until that groove is completely filled. This means that the groove will always be full of hot oil under test conditions. Similarly, the non-load carrying region in the vertical position will be full of hot oil. By the action of gravity, these two regions will feed hot oil into the inlet groove containing thermocouples 1 and 2. Verification of this state of affairs can be obtained by reviewing the observed results in Appendix IV. It will be noted that the temperatures recorded by thermocouples 1 and 2 were higher than those recorded in the other inlet grooves. Since the average temperature rise across the offending pad is very small, its load carrying capacity will be greatly impaired.

Comparison of Theoretical and Experimental Results

Referring to Figure 13, it is seen that the experimental curves tend toward the theory at medium film thicknesses, then fall away again at low film thicknesses. The main reason for the divergence at low film thicknesses lies in the inlet temperatures of the oil. In the theory, the inlet temperature was assumed constant at $70°F$, whereas average inlet temperatures of up to $150°F$ were recorded experimentally. Since the thermal wedge depends on viscosity to produce a temperature rise across the bearing and since the viscosity varies as $t^{-2.71}$, then it follows that the increased inlet temperature will reduce the load carrying capacity of the bearing. A point check was made on this by obtaining a computer solution for the load carried at 15,000 r.p.m. The load was found to be reduced from 25.30 lbs.

at 70°F to 13.85 lbs. at 100°F. These figures demonstrate the severe effect that the inlet oil temperature has on the bearing performance and explain the reduction in the load observed in the 1.0×10^{-3} to 1.75×10^{-3} range of film thickness in Figure 13.

In the film thickness range 1.75×10^{-3} to 2.5×10^{-3} the experimental load is close to the theoretical curve and actually exceeds the theory in some parts. In this range the static pressure predominates and the hydrodynamic theory does not account for the static pressure. The value of the static pressure was about 5 lbs./sq.in. but since the actual value depends on the losses in the supply line and at entry to the bearing surfaces, no attempt has been made to subtract load carried by the static pressure from the total bearing load.

For film thicknesses greater than 2.5×10^{-3} the centrifugal force becomes important. In Chapter II it was shown that the centrifugal term in the differential equation was relatively small for moderate or high hydrodynamic pressures. However, the induced pressures are low in the range in question and consequently the centrifugal force, which impairs the load carrying capacity of the bearing, becomes relatively important. The effect of the centrifugal force can be seen to extend down to film thicknesses of about 1.25×10^{-3}. For films thicker than 1.25×10^{-3} the increase in load which is predicted by the theory for an increase in speed, is more than offset by the corresponding increase in the centrifugal force. For films thinner than 1.25×10^{-3} an increase in speed produces a higher load carrying capacity for the same film thickness, as predicted by the theory.

The coefficient of friction curves shown in Figure 14 indicate that the experimental values of f are everywhere less than the theoretical predictions. The largest single factor causing this discrepancy is the increased temperature in the inlet oil. Since $f \propto \mu$, an increase in the oil

temperature would result in a decrease in the viscosity and in the coefficient of friction. At low values of film thickness, the observed bulk temperature of the inlet oil was about twice the assumed value. The viscosity would therefore be reduced by about 80%. For large values of film thickness the observed inlet temperature was $10°F$ above the assumed value, resulting in a 30% decrease in viscosity. The thermocouples were located in such a way that they would record only the bulk temperature of the inlet oil. From the previous discussion on recirculation of the lubricant it seems possible that a temperature gradient existed across the fluid film. Any such temperature gradient would produce a fluid layer adjacent to the rotating disc which would be at an even higher temperature than that observed experimentally. A local increase in temperature of this nature would cause a further decrease in viscosity and in the coefficient of friction.

Apart from viscosity considerations, $f \propto \frac{1}{W}$ so that any discrepancy in the load characteristics will influence the friction characteristics. In the film thickness range 1.0×10^{-3} to 1.75×10^{-3}, the experimental load is less than the theoretical load. For this range, the load error will therefore partially compensate for the viscosity error. In the range 1.75×10^{-3} to 2.5×10^{-3} it was observed that, due to the effect of static pressure, the experimental load exceeded the theoretical value. In this case the two errors are cumulative. For film thicknesses greater than 2.5×10^{-3} the experimental load is again less than the theoretical value, due to the action of centrifugal force, so that a partial correction is once more obtained.

The theory predicts that an increase in speed will be accompanied by a reduction in the coefficient of friction. In Figure 14 it will be noticed that the converse is true for film thicknesses greater than 1.25×10^{-3}. This contradiction of the theory may be attributed to the adverse influence of centrifugal force on load capacity, which has been

previously discussed, and the dependence of the coefficient of friction on the load.

Correlation of Experimental Data

The coefficient of friction has been plotted against the parameter $\frac{ZN}{P'}$ in Figure 15. The experimental results obtained are for the most part in a different range from the existing published results. The difference in range can be attributed to the low loads carried in the present series of tests and the corresponding high value of viscosity. In the region of overlap, the experimental results are close to those obtained by Young and Fogg, although the gradient of the friction curve is closer to that obtained by Kettleborough.

The wide scatter in the experimental results as obtained by different authors is probably produced by the difference in operating speeds. In section II.3 it was pointed out that for a given load carrying capacity, a lower coefficient of friction could be obtained by operating at higher speeds. That is, for two identical bearings carrying identical loads, but operating at different speeds, a lower coefficient of friction will be obtained from the bearing which runs at the higher speed. For the same inlet oil temperatures, the outlet temperatures will be the same so that the viscosity Z will be the same for the two bearings. This means that the high speed bearing will not only have a lower coefficient of friction, but it will have a higher value of $\frac{ZN}{P'}$. The friction characteristics of the two bearings will therefore differ if plotted on Figure 15.

A method of obtaining a more general correlation of experimental data is indicated by combining equations (46) and (47):

$$f = \frac{\mu' \omega}{P' h} r_m$$

$$\text{i.e. } f \propto \frac{ZN}{P'} \frac{r_m}{h} \qquad \qquad \cdot \qquad \cdot \qquad (49)$$

Equation (49) shows that a general curve could be obtained by plotting the coefficient of friction against the parameter $\frac{ZN}{P'}\frac{r_m}{h}$. Unfortunately, Fogg and Kettleborough do not give sufficient data to permit such a correlation to be made.

CHAPTER V

V.1. Summary and Conclusions

The existence of a load carrying fluid film due to the action of a thermal wedge has been demonstrated both theoretically and experimentally. In both theory and experiment it was found that the maximum temperature of the lubricant reached restrictive values before the film thickness was reduced to undesirable limits.

Theoretically, it seems possible for a parallel surface thrust bearing to support hydrodynamic loads of the order of 30 lbs./sq.in. of bearing area. In general, it can be concluded that for a given load capacity a high operating speed is associated with a low coefficient of friction.

Experimentally, loads of about 12 lbs./sq.in. of bearing area were supported. This load carrying capacity is considerably less than that obtained by other investigators. The factor which limited the load capacity of the bearing was recirculation of the lubricant which resulted in high inlet temperatures to the bearing. In this respect the existence of separate oil outlet grooves for each thrust pad appear to be of little or no value and if used in certain configurations they can have a detrimental effect. The friction characteristics obtained are in good agreement with the results obtained by other experimenters.

V.2. Suggestions for Future Reasearch

It would seem desirable to attempt to develop the load carrying capacity of the parallel surface thrust bearing before performing any further tests. In this respect it seems necessary to restrict the radial flow of oil at the periphery of the bearing to ensure an adequate supply of lubricant reaches all areas of the bearing surfaces. One method of achieving this is to fit circumferential seals as described by Fogg. The seals used by Fogg were $\frac{1}{4}$ inch thick and had a diametral clearance of 0.010 inch.

Alternatively, the same effect could be achieved by reversing the oil flow so that the oil enters the bearing at the outer radius and leaves at the inner radius. With this type of flow, the radial oil grooves could be wedge shaped which would allow for the proper flow of oil into the bearing and at the same time conveniently furnish sector shaped thrust pads.

To permit accurate experimental values of the coefficient of friction to be obtained, the bearing torque must be accurately known. For small, high speed bearings, the friction torque is low and the weight pan method of obtaining the bearing torque is rather insensitive. Considerable improvement in sensitivity could be obtained by employing a small force transducer to act on the torque arm. In this way rapid torque readings could be obtained with a high degree of accuracy.

Finally, an automatic shut-down device could be installed which would permit tests to be made in the thin film region. A relay switch for the main motor could be fitted to the bearing assembly in such a way that if metal to metal contact occurs, the resulting increased friction torque would cause the torque arm to depress the relay button and so stop the main motor.

APPENDICES

APPENDIX I

The Energy Equation in Lubrication.

Two different forms of energy equation are to be found in the literature - for example, the equation used by Cope [6] differs from that used by Christopherson [9]. In Chapter II, the energy equation obtained agrees with that obtained by Christopherson. The reason for this will be shown by repeating the procedure of Chapter II and at the same time repeating Cope's derivation. In the following analysis, equations and assumption numbers with the subscript 'a' will refer to Cope's analysis. To permit direct comparison with Cope's results, rectangular co-ordinates will be used.

For the steady, laminar flow of a Newtonian fluid we had:

$$\left(\rho u \frac{\partial H}{\partial x} + \rho v \frac{\partial H}{\partial y} + \rho w \frac{\partial H}{\partial z}\right) = \left(u \frac{\partial p}{\partial x} + v \frac{\partial p}{\partial y} + w \frac{\partial p}{\partial z}\right) + \frac{\partial}{\partial x}\left(k \frac{\partial t}{\partial x}\right) + \frac{\partial}{\partial y}\left(k \frac{\partial t}{\partial y}\right) + \frac{\partial}{\partial z}\left(k \frac{\partial t}{\partial z}\right) + \phi$$

$$\text{but} \quad H = E + \frac{p}{\rho}$$

Substituting this expression into the previous equation, we get:

$$\left(\rho u \frac{\partial E}{\partial x} + \rho v \frac{\partial E}{\partial y} + \rho w \frac{\partial E}{\partial z}\right) - \frac{p}{\rho}\left(u \frac{\partial \rho}{\partial x} + v \frac{\partial \rho}{\partial y} + w \frac{\partial \rho}{\partial z}\right) = \frac{\partial}{\partial x}\left(k \frac{\partial t}{\partial x}\right) + \frac{\partial}{\partial y}\left(k \frac{\partial t}{\partial y}\right) + \frac{\partial}{\partial z}\left(k \frac{\partial t}{\partial z}\right) + \phi$$

but from the continuity equation,

$$u \frac{\partial \rho}{\partial x} + v \frac{\partial \rho}{\partial y} + w \frac{\partial \rho}{\partial z} = -\rho\left(\frac{\partial u}{\partial x} + \frac{\partial v}{\partial y} + \frac{\partial w}{\partial z}\right)$$

Substituting this expression in the above equation we get:

$$\left(\rho u \frac{\partial E}{\partial x} + \rho v \frac{\partial E}{\partial y} + \rho w \frac{\partial E}{\partial z}\right) + p\left(\frac{\partial u}{\partial x} + \frac{\partial v}{\partial y} + \frac{\partial w}{\partial z}\right) = \frac{\partial}{\partial x}\left(k \frac{\partial t}{\partial x}\right) + \frac{\partial}{\partial y}\left(k \frac{\partial t}{\partial y}\right) + \frac{\partial}{\partial z}\left(k \frac{\partial t}{\partial z}\right) + \phi$$

Thus we have two identical forms of the energy equation,

$$\left(\rho u \frac{\partial H}{\partial x} + \rho v \frac{\partial H}{\partial y} + \rho w \frac{\partial H}{\partial z}\right) - \left(u \frac{\partial p}{\partial x} + v \frac{\partial p}{\partial y} + w \frac{\partial p}{\partial z}\right) = \frac{\partial}{\partial x}\left(k \frac{\partial t}{\partial x}\right) + \frac{\partial}{\partial y}\left(k \frac{\partial t}{\partial y}\right) + \frac{\partial}{\partial z}\left(k \frac{\partial t}{\partial z}\right) + \phi \quad \cdot \quad (50)$$

$$\left(\rho u \frac{\partial E}{\partial x} + \rho v \frac{\partial E}{\partial y} + \rho w \frac{\partial E}{\partial z}\right) + p\left(\frac{\partial u}{\partial x} + \frac{\partial v}{\partial y} + \frac{\partial w}{\partial z}\right) = \frac{\partial}{\partial x}\left(k \frac{\partial t}{\partial x}\right) + \frac{\partial}{\partial y}\left(k \frac{\partial t}{\partial y}\right) + \frac{\partial}{\partial z}\left(k \frac{\partial t}{\partial z}\right) + \phi \quad \cdot \quad (50a)$$

The second of these equations was obtained by Cope.

As before, we assume

(i) That p, ρ, t, μ and k are functions of x and y only

(ia) That p, ρ, t, μ and k are functions of x and y only

(ii) That $\frac{\partial u}{\partial \mathfrak{z}} \gg \frac{\partial u}{\partial x}$, $\frac{\partial^2 u}{\partial \mathfrak{z}^2} \gg \frac{\partial^2 u}{\partial \mathfrak{z} \partial x} \gg \frac{\partial^2 u}{\partial x^2}$ and so on

(iia) That $\frac{\partial u}{\partial \mathfrak{z}} \gg \frac{\partial u}{\partial x}$, $\frac{\partial^2 u}{\partial \mathfrak{z}^2} \gg \frac{\partial^2 u}{\partial \mathfrak{z} \partial x} \gg \frac{\partial^2 u}{\partial x^2}$ and so on

(iii) That $w = 0$

(iiia) That $w = 0$

(iv) That $H = C_p t$

(iva) That $E = C_v t$

Applying these assumptions, the equations become:

$$\left(\rho C_p u \frac{\partial t}{\partial x} + \rho C_p v \frac{\partial t}{\partial y} \right) - \left(u \frac{\partial p}{\partial x} + v \frac{\partial p}{\partial y} \right) = \frac{\partial}{\partial x} \left(k \frac{\partial t}{\partial x} \right) + \frac{\partial}{\partial y} \left(k \frac{\partial t}{\partial y} \right) + \mu \left[\left(\frac{\partial u}{\partial \mathfrak{z}} \right)^2 + \left(\frac{\partial v}{\partial \mathfrak{z}} \right)^2 \right] \qquad \cdot \quad (51)$$

$$\left(\rho C_v u \frac{\partial t}{\partial x} + \rho C_v v \frac{\partial t}{\partial y} \right) + p \left(\frac{\partial u}{\partial x} + \frac{\partial v}{\partial y} \right) = \frac{\partial}{\partial x} \left(k \frac{\partial t}{\partial x} \right) + \frac{\partial}{\partial y} \left(k \frac{\partial t}{\partial y} \right) + \mu \left[\left(\frac{\partial u}{\partial \mathfrak{z}} \right)^2 + \left(\frac{\partial v}{\partial \mathfrak{z}} \right)^2 \right] \qquad \cdot \quad (51a)$$

Next, we make a term by term appraisal and hence assume that:

(v) conductivity terms $\left[\frac{\partial}{\partial x} \left(k \frac{\partial t}{\partial x} \right) \, etc. \right]$ are negligible

(va) conductivity terms $\left[\frac{\partial}{\partial x} \left(k \frac{\partial t}{\partial x} \right) \, etc. \right]$ are negligible

(via) dilation terms $p \left(\frac{\partial u}{\partial x} \, etc. \right)$ are negligible

With these assumptions we get:

$$\left(\rho C_p u \frac{\partial t}{\partial x} + \rho C_p v \frac{\partial t}{\partial y} \right) = \left(u \frac{\partial p}{\partial x} + v \frac{\partial p}{\partial y} \right) + \mu \left[\left(\frac{\partial u}{\partial \mathfrak{z}} \right)^2 + \left(\frac{\partial v}{\partial \mathfrak{z}} \right)^2 \right] \qquad \cdot \qquad \cdot \quad (52)$$

$$\left(\rho C_v u \frac{\partial t}{\partial x} + \rho C_v v \frac{\partial t}{\partial y} \right) = \mu \left[\left(\frac{\partial u}{\partial \mathfrak{z}} \right)^2 + \left(\frac{\partial v}{\partial \mathfrak{z}} \right)^2 \right] \qquad \cdot \qquad \cdot \quad (52a)$$

Finally, we apply the velocity distribution expressions,

$$u = -\frac{1}{2\mu} \frac{\partial p}{\partial x} \mathfrak{z} (h - \mathfrak{z})$$

$$v = -\frac{1}{2\mu} \frac{\partial p}{\partial y} \mathfrak{z} (h - \mathfrak{z}) + \frac{U}{h} (h - \mathfrak{z})$$

and integrate with respect to $\mathfrak{z}$ between the limits of $\mathfrak{z} = 0$ and $\mathfrak{z} = h$. These

steps result in the equations:

$$\rho C_p \left[\left(\frac{Uh}{2} - \frac{h^3}{12\mu} \frac{\partial p}{\partial x} \right) \frac{\partial t}{\partial x} - \left(\frac{h^3}{12\mu} \frac{\partial p}{\partial y} \right) \frac{\partial t}{\partial y} \right] = \frac{\mu U^2}{h} + \frac{Uh}{2} \frac{\partial p}{\partial x} \qquad \cdot \qquad \cdot \quad (53)$$

$$\rho C_v \left[\left(\frac{Uh}{2} - \frac{h^3}{12\mu} \frac{\partial p}{\partial x} \right) \frac{\partial t}{\partial x} - \left(\frac{h^3}{12\mu} \frac{\partial p}{\partial y} \right) \frac{\partial t}{\partial y} \right] = \frac{\mu U^2}{h} + \frac{h^3}{12\mu} \left[\left(\frac{\partial p}{\partial x} \right)^2 + \left(\frac{\partial p}{\partial y} \right)^2 \right] \qquad \cdot \quad (53a)$$

The first of these equations is the cartesian form of the energy equation

obtained in Chapter II. Equation (53a) was obtained by Cope and was later

supported by Charnes, Osterle and Saibel [13]. However, the latter authors

used the Reynolds' equation in their derivation and Reynolds, in turn, used

the concept of volume continuity as opposed to mass continuity.

Apart from being a little more accurate than equation (53a), equation (53) has the advantage of being somewhat simpler. Furthermore, equation (53) involves the specific heat at constant pressure which is more readily obtainable than that at constant volume.

APPENDIX II

Physical Properties of Shell Turbo 27 Oil

The density and viscosity of the lubricant have to be known functions of temperature to permit a solution of the governing equations. Consequently, tests were carried out to obtain an accurate graphical relationship between these quantities and the temperature. Viscosities were measured using a Saybolt Universal Viscometer and densities were measured using a hydrometer. The results are shown graphically in Figure 16. The curves:

$$\rho = \left(1.727 - 0.000686\, t \right)\ lbs.\,sec.^2 / ft^4 \tag{54}$$

$$\mu = 152\ t^{-2.71}\ lbs.\,sec.^2 / ft^2 \tag{55}$$

fit the experimental curves to within 1% in the temperature range encountered. The specific heat was assumed constant at the value supplied by the Shell Oil Company Ltd.

$$C_p = 0.497\ Btu / lb.\,^{\circ}F$$
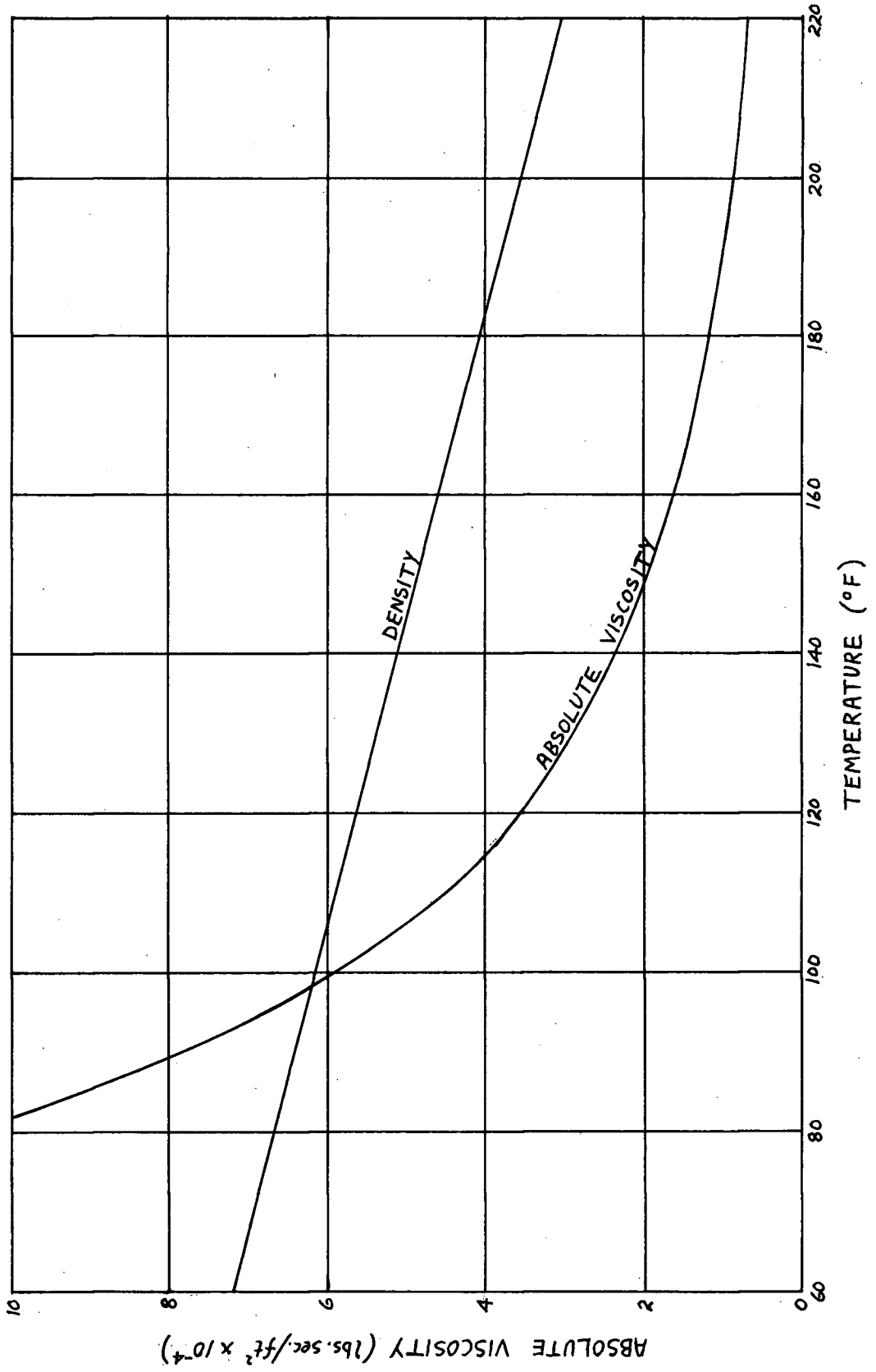
FIG.16 PHYSICAL PROPERTIES OF SHELL TURBO 27 OIL

APPENDIX III

Calibration Tests on Apparatus

Calibration tests were carried out to determine, (1) the temperature versus emf characteristic for the thermocouples and (2) the loading pressure versus applied load curve for the loading system.

Thermocouple Calibration

The emf characteristic of the thermocouples was obtained by a check at the steam point. This was done by placing the hot junction in a hypsometer and the cold junction in a flask containing water and crushed ice at the melting point. In this manner the emf was measured as 4.258 mV with the barometer reading 739.8 mm of mercury. From this information the evaporation temperature of the steam was calculated from the relation:

$$t_p = t_{760} + 36.8578\left(\frac{p_b-760}{1000}\right) - 20.159\left(\frac{p_b-760}{1000}\right)^2 + 16.21\left(\frac{p_b-760}{1000}\right)^3$$

where t_p = temperature of wet steam at pressure p, in °C

t_{760} = 100.00 °C

p_b = barometric pressure, in mm of mercury

Thus the saturation temperature was calculated to be 210.64°F and from standard tables, derived from Adam's Tables, the emf for this temperature is found to be 4.241 mV. This deviation of 0.4% was assumed to be linearly distributed from the steam point to the ice point, so that the curve shown in Figure 17 was obtained.

Loading System Calibration

To obtain a relation between the pressure applied to the loading jacks and the load delivered to the thrust surfaces, an in-site loading test was made. The high speed shaft was removed from the test bearing and the piston tubes sealed so that the space between the two opposing pistons was pressure tight. The oil outlet was then utilized to

admit pressurized oil from a gauge tester into this space. Thus a known

pressure could be applied to the loading jacks by one gauge tester and a

known pressure applied to the thrust pad faces by another tester. The

complete drive system up to and including the gear box was then started up

and a series of pressure readings taken for zero piston motion. This

enabled the loading curve of Figure 18 to be drawn, from which the maximum

deviation was found to be 5%.
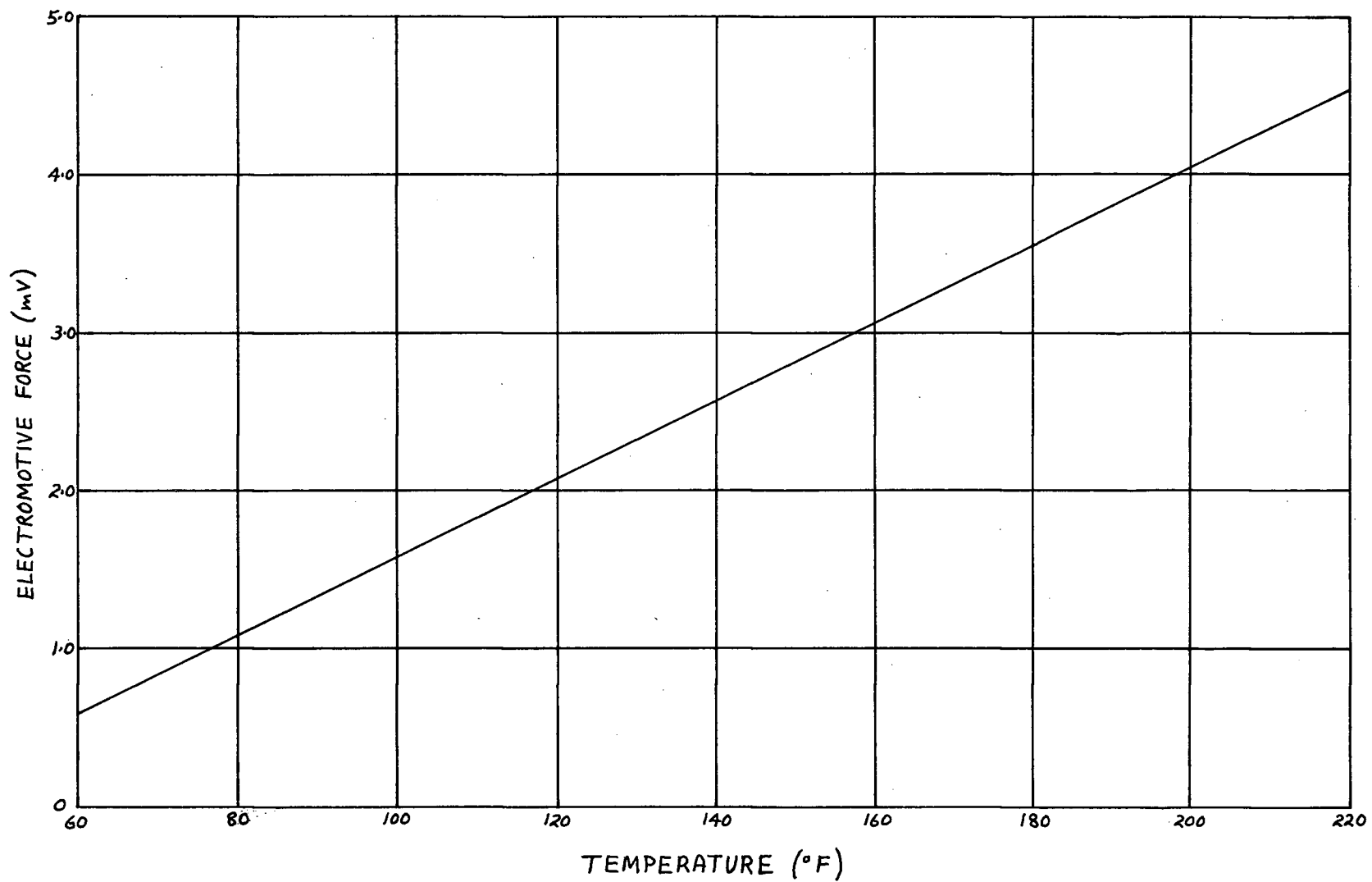
FIG. 17 CALIBRATION CURVE FOR COPPER-CONSTANTAN THERMOCOUPLES

PRESSURE APPLIED TO LOADING JACKS (lbs./in²)

TOTAL BEARING LOAD (lbs.)
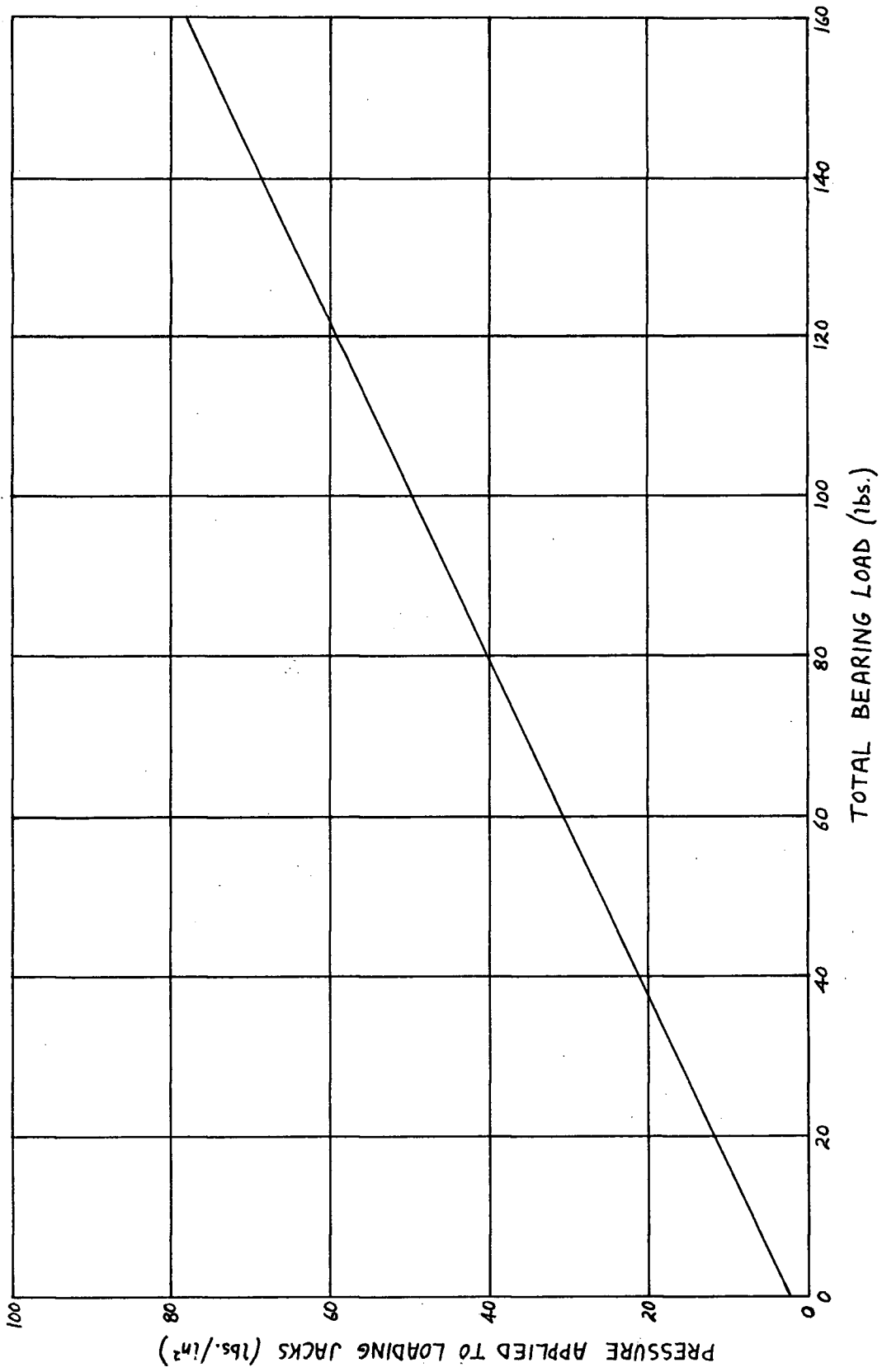
FIG. 18 CALIBRATION CURVE FOR LOADING SYSTEM

APPENDIX IV

The observed experimental results are presented in Tables III to VII. In these Tables, the following symbols have been used:

p_L = loading pressure applied to hydraulic loading jacks (lbs./sq.in.)

h_1 = film thickness reading (ins x 10^{-3})

h_2 = zero reading with bearing components hot (ins x 10^{-3})

Q = oil flow collected in time $\delta t'$ (c.c.)

$\delta t'$ = time interval to collect oil flow Q (secs.)

W_T = weight applied to torque arm at 10 inch radius (ozs.)

e_n = thermocouple e.m.f. for position indicated by subscript (mV)

t_b = bulk oil outlet termperature (°F)

The thermocouple positions are shown in Figure 7.

TABLE III   SPEED=15,000 r.p.m.

p_L	h_1	h_2	Q	$\delta t'$	W_T	e_1	e_2	e_3	e_4	e_5	e_6	e_7	e_8	e_9	e_{10}	e_{11}	e_{12}	t_b
5	3.10	0.09	355	9.2	11.5	1.70	1.97	1.86	2.02	1.11	1.68	1.67	2.02	1.07	1.44	1.62	2.00	124
10	2.80	0.09	405	11.6	12.0	1.87	2.08	1.98	2.14	1.17	1.70	1.73	2.13	1.14	1.49	1.69	2.11	128
15	2.43	0.10	400	14.1	12.5	2.10	2.35	2.18	2.42	1.35	1.96	1.92	2.37	1.28	1.73	1.94	2.36	137
20	1.48	0.12	405	27.4	9.0	2.65	3.31	3.00	3.33	1.96	3.03	2.74	3.23	1.86	2.72	2.98	3.35	168
25	1.05	0.14	390	43.8	7.5	3.37	4.34	3.82	4.21	2.75	3.95	3.64	4.12	2.61	3.62	3.91	4.26	192

TABLE IV   SPEED=15,900 r.p.m.

p_L	h_1	h_2	Q	$\delta t'$	W_T	e_1	e_2	e_3	e_4	e_5	e_6	e_7	e_8	e_9	e_{10}	e_{11}	e_{12}	t_b
5	2.95	0.11	297	8.0	9.5	1.70	2.09	1.98	2.13	1.10	1.77	1.76	2.12	1.04	1.50	1.78	2.12	123
10	2.69	0.11	307	9.5	12.5	1.93	2.23	2.07	2.24	1.17	1.77	1.83	2.14	1.12	1.53	1.79	2.21	130
15	2.25	0.12	285	9.8	12.0	2.14	2.48	2.32	2.51	1.30	1.90	2.00	2.21	1.23	1.73	2.00	2.45	139
20	1.48	0.15	255	15.4	9.0	2.58	3.26	3.00	3.34	1.86	2.86	2.67	3.18	1.73	2.63	2.89	3.30	164
25	1.15	0.16	275	24.4	8.5	3.00	4.00	3.58	3.95	2.34	3.57	3.31	3.79	2.21	3.22	3.54	3.93	180

TABLE V

SPEED=17,000 r.p.m.

p_L	h_1	h_2	Q	$\delta t'$	W_T	e_1	e_2	e_3	e_4	e_5	e_6	e_7	e_8	e_9	e_{10}	e_{11}	e_{12}	t_b
5	2.85	0.11	310	7.6	10.5	1.60	2.08	2.00	2.15	1.10	1.74	1.76	2.12	1.05	1.42	1.74	2.12	122
10	2.60	0.11	345	9.2	12.5	1.86	2.22	2.10	2.24	1.17	1.75	1.82	2.21	1.12	1.50	1.79	2.19	131
15	2.20	0.12	292	9.0	13.0	2.09	2.54	2.40	2.60	1.36	2.07	2.05	2.52	1.31	1.85	2.09	2.56	141
20	1.42	0.14	313	16.4	9.0	2.54	3.42	3.10	3.42	1.83	2.89	2.75	2.73	1.76	2.70	3.00	3.40	164

TABLE VI

SPEED=18,100 r.p.m.

p_L	h_1	h_2	Q	$\delta t'$	W_T	e_1	e_2	e_3	e_4	e_5	e_6	e_7	e_8	e_9	e_{10}	e_{11}	e_{12}	t_b
5	2.65	0.10	635	14.8	9.0	1.54	2.15	2.06	2.19	1.12	1.74	1.83	2.19	1.05	1.48	1.82	2.16	123
10	2.42	0.10	460	11.5	12.0	1.81	2.28	2.19	2.33	1.15	1.73	1.90	2.31	1.10	1.53	1.86	2.28	133
15	2.05	0.11	345	11.0	12.0	2.05	2.60	2.45	2.59	1.31	2.00	2.10	2.55	1.24	1.78	2.08	2.55	145
20	1.40	0.13	365	16.0	9.0	2.40	3.21	2.99	3.28	1.66	2.59	2.56	3.13	1.58	2.38	2.76	2.23	168

TABLE VII

SPEED=19,100 r.p.m.

p_L	h_1	h_2	Q	$\delta t'$	W_T	e_1	e_2	e_3	e_4	e_5	e_6	e_7	e_8	e_9	e_{10}	e_{11}	e_{12}	t_b
5	2.60	0.12	424	9.6	9.5	1.49	2.23	2.14	2.29	1.14	1.80	1.85	2.25	1.09	1.52	1.89	2.23	127
10	2.40	0.13	345	8.0	12.5	1.81	2.35	2.22	2.39	1.18	1.79	1.94	2.34	1.13	1.53	1.93	2.31	133
15	2.05	0.14	295	8.4	13.0	2.00	2.62	2.50	2.66	1.30	2.10	2.13	2.62	1.28	1.78	2.19	2.62	145
20	1.43	0.16	210	8.8	9.0	2.29	3.24	3.00	3.25	1.66	2.65	2.58	3.19	1.55	2.38	2.79	3.19	167

<u>BIBLIOGRAPHY</u>

[1] Reynolds, O.   "On the Theory of Lubrication and Its Application
                                to Mr. Beauchamp Tower's Experiments", Phil. Trans.
                                of the Roy. Soc. of London, vol. 177, 1886.

[2] Fogg, A.   "Fluid Film Lubrication of Parallel Thrust
                                Surfaces", Proc. Inst. Mech. Engrs., vol. 155,
                                1946.

[3] Bower, G.S.   Contribution to Fogg [2]

[4] Cameron, A. and Wood, W.L.
                                "Parallel Surface Thrust Bearings", Proc. 6th.
                                Inter. Cong. of App. Mech., 1946.

[5] Shaw, M.C.   "An Analysis of the Parallel Surface Thrust
                                Bearing", Trans. Amer. Soc. Mech. Engrs. vol. 69,
                                1947.

[6] Cope, W.F.   "The Hydrodynamical Theory of Film Lubrication",
                                Proc. Roy. Soc., series A, vol. 197, 1949.

[7] Kettleborough, C.F.   "Tests on Parallel Surface Thrust Bearings",
                                Engineering, Aug. 1955.

[8] Young, J.   "The Thermal Wedge Effect in Hydrodynamic
                                Lubrication", Engineering Journal, vol. 45,
                                number 3, 1962.

[9] Christopherson, D.G.   "A New Mathematical Method for the Solution of
                                Film Lubrication Problems", Proc. Inst. Mech.
                                Engrs., vol. 146, 1942.

[10] Bird, R.B., Stewart, W.E., and Lightfoot, E.N.
                                "Transport Phenomena", John Wiley & Sons, Inc.,
                                1960.

[11] Southwell, R.V.   "Relaxation Methods in Engineering Science",
                                Clarendon Press, Oxford, 1940.

[12] Christopherson, D.G., and Southwell, R.V.
                                "Relaxation Methods Applied to Engineering
                                Problems", Proc. Roy. Soc., series A, vol. 168,
                                1938.

[13] Charnes, A., Osterle, F., and Saibel, E.
                                "On the Energy Equation for Fluid-Film
                                Lubrication", Proc. Roy. Soc., series A, vol. 214,
                                1952.